J. Fluid Mech. (2013), *vol.* 735, *pp.* 307–346. © Cambridge University Press 2013
doi:10.1017/jfm.2013.469

Flow past a rotationally oscillating cylinder

S. Kumar[1],†, C. Lopez[1], O. Probst[2], G. Francisco[1], D. Askari[1] and Y. Yang[1]

[1]School of Engineering and Computational Science, The University of Texas at Brownsville, Brownsville, TX 78520, USA

[2]Physics Department, Instituto Tecnológico y de Estudios Superiores de Monterrey, Monterrey, Mexico

(Received 17 May 2012; revised 7 July 2013; accepted 4 September 2013;
first published online 24 October 2013)

Flow past a circular cylinder executing sinusoidal rotary oscillations about its own axis is studied experimentally. The experiments are carried out at a Reynolds number of 185, oscillation amplitudes varying from $\pi/8$ to π, and at non-dimensional forcing frequencies (ratio of the cylinder oscillation frequency to the vortex-shedding frequency from a stationary cylinder) varying from 0 to 5. The diagnostic is performed by extensive flow visualization using the hydrogen bubble technique, hot-wire anemometry and particle-image velocimetry. The wake structures are related to the velocity spectra at various forcing parameters and downstream distances. It is found that the phenomenon of lock-on occurs in a forcing frequency range which depends not only on the amplitude of oscillation but also the downstream location from the cylinder. The experimentally measured lock-on diagram in the forcing amplitude and frequency plane at various downstream locations ranging from 2 to 23 diameters is presented. The far-field wake decouples, after the lock-on at higher forcing frequencies and behaves more like a regular Bénard–von Kármán vortex street from a stationary cylinder with vortex-shedding frequency mostly lower than that from a stationary cylinder. The dependence of circulation values of the shed vortices on the forcing frequency reveals a decay character independent of forcing amplitude beyond forcing frequency of $\sim$1.0 and a scaling behaviour with forcing amplitude at forcing frequencies $\leqslant$1.0. The flow visualizations reveal that the far-field wake becomes two-dimensional (planar) near the forcing frequencies where the circulation of the shed vortices becomes maximum and strong three-dimensional flow is generated as mode shape changes in certain forcing parameter conditions. It is also found from flow visualizations that even at higher Reynolds number of 400, forcing the cylinder at forcing amplitudes of $\pi/4$ and $\pi/2$ can make the flow field two-dimensional at forcing frequencies greater than $\sim$2.5.

Key words: vortex shedding, vortex streets, wakes

1. Introduction

The study of flow past bluff bodies executing forced motions is important for engineering applications such as problems related to flow-induced vibrations and flow control. In addition, such flows offer the opportunity to study the basic underlying physics of the flow phenomena. The circular cylinder offers a very simple geometry

† Email address for correspondence: Sanjay.Kumar@utb.edu

https://doi.org/10.1017/jfm.2013.469 Published online by Cambridge University Press

for studies in bluff body flows. The flow around a circular cylinder has been studied for over a century and a comprehensive account of this can be found in the review article by Williamson (1996). The addition of periodic forcing to a bluff body such as a circular cylinder produces interesting effects on the wake. One of the interesting effects is the phenomenon of lock-on. This refers to the situation when the vortex-shedding frequency in the wake is the same as the forcing frequency of the bluff body such as a circular cylinder. Forcing of the cylinder can be induced in several ways including oscillating the cylinder in-line or transverse to the flow direction. Such phenomena are reported in the works of Bishop & Hassan (1964), Tanida, Okajima & Watanabe (1973), Griffin & Ramberg (1976) and Hurlbut, Spaulding & White (1982). Review articles by Berger & Willie (1972) and Bearman (1984) give accounts of some properties of such forced flows.

Flow past a circular cylinder executing rotational oscillations about its own axis has not been as widely studied as in-line or transverse oscillations, at least from the point of view of lock-on. The phenomenon of lock-on using rotational oscillations was first studied by Okajima, Takata & Asanuma (1975). They studied the problem numerically in the Reynolds number range from 40 to 80 and experimentally in the range from 80 to 6100 using only one velocity amplitude (the ratio of the maximum cylinder surface velocity to free stream velocity) which resulted in limited or no wake structure effects. The Reynolds number, Re, here is defined as $Re = U_\infty D/\nu$, where U_∞ is the free-stream velocity, D the cylinder diameter and ν the kinematic viscosity. Taneda (1978) experimentally studied flow past a rotationally oscillating circular cylinder using flow visualization methods in the Re range from 30 to 300, oscillation amplitudes ranged from 30° to 90° and forcing frequencies varied over a wide range. The observations were however confined very close to the cylinder ($\sim$2–3D) and the lock-on phenomenon was not studied in detail.

Badr & Dennis (1985) conducted a two-dimensional numerical study of a cylinder started impulsively in both translatory and rotary motion in a viscous incompressible fluid. The computations were performed at $Re \geqslant 200$. The focus of the work was however confined to the time development of the separated flow at $Re = 200$. Lu & Sato (1996) found using two-dimensional computations at $Re = 200$, 1000 and 3000 that the large-scale structures near the cylinder were not strongly affected by the Reynolds number. Baek & Hyung (1998) numerically studied the initial vortex formation process at oscillation amplitudes of 15, 30 and 60° and forcing frequencies near the lock-on range at $Re = 110$. They observed a change in mode shape near the forcing frequency equal to the natural vortex-shedding frequency from a stationary cylinder. Similar behaviour was also observed by Dennis, Nguyen & Kocabiyik (2000) in their two-dimensional numerical simulations of a rotationally oscillating and translating cylinder at $Re = 500$ and 1000.

Tokumaru & Dimotakis (1991) conducted an experimental study on flow past a cylinder executing rotary oscillations at $Re = 15\,000$. The forcing velocity amplitudes varied from 0 to 16 and forcing Strouhal number (forcing frequency normalized by cylinder diameter and free stream velocity) from 0.17 to 3.3. Their flow visualizations and wake profile measurements have shown that significant control on wake structure can be achieved by such oscillatory forcing. They found that maximum control on the wake structure can be achieved when vortices are shed near the forcing frequency, i.e. near lock-on. They found a significant reduction in drag coefficient ($\sim$80 %) near a forcing Strouhal number between 0.8 and 1.0 and velocity amplitude of 2.0. This seminal study was, however, at much higher Reynolds number compared with the present work at $Re = 185$ and did not focus on providing the spatial variation of the

https://doi.org/10.1017/jfm.2013.469 Published online by Cambridge University Press

wake structure such as its frequency content and mode evolution. The reduction in drag reported by Tokumaru & Dimotakis (1991) and some other flow features were later numerically validated by the two-dimensional computations of He *et al.* (2000) and Shiels & Leonard (2001). Shiels & Leonard (2001) also showed that the technique of rotationally oscillating cylinder is not effective for drag reduction at relatively lower Reynolds numbers; however, Bergmann, Cordier & Brnacher (2006) have shown that by imparting rotational oscillations on only selected upstream portion of the cylindrical surface similar drag reduction can be obtained at much lower $Re = 200$. Tokumaru & Dimotakis (1993) further studied the problem with rotary oscillations superposed on steady rotation. Their focus was on studying the mean lift coefficient on a cylinder executing such motions. They found that for steady rotations, larger aspect ratio cylinders yield much higher lift coefficients than that proposed by Prandtl (1925). The addition of rotary oscillations to steady rotations was found to increase the lift in some cases.

Fujisawa, Kawaji & Ikemoto (2001) conducted an experimental study of vortex-shedding control from a circular cylinder using rotary oscillations at $Re = 6700$ and 20 000 using hot-wire anemometry and smoke-wire flow visualization. They employed a feedback mechanism using the velocity signal from the separated shear layer to control the cylinder oscillations resulting in reduced drag compared with a stationary cylinder. Similar work was numerically done by Lu, Qin & Li (2011) who proposed an active flow control technique for rotationally oscillating cylinder using the real-time lift coefficient as a feedback signal in the Re range from 60 to 200. Fujisawa, Tanahashi & Srinivas (2005), in their experimental study, investigated the pressure field and fluid forces on a rotationally oscillating cylinder at $Re = 2000$ and found a drag reduction of $\sim 30\,\%$. Lee & Lee (2006) experimentally studied the flow past a rotationally oscillating cylinder at $Re = 4140$, oscillation amplitudes ranging from 0 to 60°, and forcing frequency ratio, F_R, varying from 0 to 2. Here F_R is defined as the ratio of forcing frequency to the vortex-shedding frequency from a stationary cylinder (Strouhal frequency). The lock-on was always found to occur at $F_R = 1$ and the lock-on region expanded with increasing amplitude. They also found drag reduction when F_R was less than 1 at fixed oscillation amplitude of 30°. Their second study (Lee & Lee 2008) was limited to one oscillation amplitude of 30° and F_R in the range from 0 to 1.6. They divided the near wake into three regimes: non-lock-on, transitional and lock-on depending on F_R.

Thiria, Goujon-Durand & Wesfreid (2006) experimentally studied the wake of a circular cylinder performing rotary oscillations using planar laser-induced fluorescence flow visualization and particle-image velocimetry (PIV) at a Reynolds number of 150. They found that wake structure is strongly affected by forcing parameters. They showed that the wake is composed of a lock-on region where vortices are shed at the forcing frequency and a region where vortices are reorganized to give a shedding frequency close to that for an unforced cylinder. They studied the implications of wake-structure modification on the mean flow properties and its direct impact on drag. For the first time, they directly measured the drag for the oscillating cylinder and correlated the drag modification with the injection of external vorticity. Similar results on mean drag modifications were also obtained numerically by Protas & Wesfreid (2002) at the same Re. Thiria & Wesfreid (2007) again studied the same problem with focus on stability characteristics. They performed linear stability analysis of the forced flow and showed that the stability characteristics are governed by the mean flow correction due to forcing. These studies studied lock-on from the linear stability characteristics point of view but the detailed spatial evolution of wake frequency

https://doi.org/10.1017/jfm.2013.469 Published online by Cambridge University Press

content and its relation to lock-on was not extensively discussed and it was also assumed that the wake would behave in a two-dimensional manner at all forcing parameters which is shown in the present work to be not true. The studies of Thiria *et al.* (2006) and Thiria & Wesfreid (2007) are closest to the present study and also provide theoretical framework to some aspects of the work discussed here.

Mahfouz & Badr (2000) investigated the unsteady flow characteristics in the wake of a rotationally oscillating cylinder using two-dimensional computations. They studied the Re range from 40 to 200, oscillation amplitudes from 0 to π and F_R from 0 to 2. They found that lock-on phenomenon occurs within a band of forcing frequencies that include the Strouhal frequency. This band depends strongly on amplitude and becomes wider as oscillation amplitude increases. A qualitative frequency selection diagram was provided in the forcing amplitude/frequency plane. However, no attempt was made to find the lock-on region in that plane. Similar numerical work was reported by Cheng, Chew & Luo (2001) at $Re = 1000$ in the near wake ($\sim 5D$ downstream extent) and by Choi, Choi & Kang (2002) at $Re = 100$.

The wake of a rotationally oscillating cylinder evolves spatially (Thiria & Wesfreid 2007) and can potentially develop three-dimensionalities depending on the forcing parameters and the global two-dimensional wake structure. The numerical work reported so far was only confined to two-dimensional studies and the experimental data confined to a plane. There is very little work studying the three-dimensional aspects of the flow past a cylinder executing rotary oscillations. The only studies of which the authors are aware are the computational studies by Poncet (2002, 2004), Deng, Shao & Ren (2007) and Jacono *et al.* (2010). Poncet (2002) showed that at $Re = 500$ a rotation at high enough amplitude makes the three-dimensional instabilities (mode B) vanish and makes the flow nominally two-dimensional. This was demonstrated for two values of forcing frequencies. Similar results were shown by Deng *et al.* (2007). In the second study, Poncet (2004) studied the flow behind a cylinder started impulsively in rectilinear motion and then executing rotational oscillations. He showed that at $Re = 400$ the flow returns to its nominal two-dimensional state when the amplitude and frequency are high enough (forcing amplitude $= \pi/2$ and $F_R = 2$) and this also resulted in decrease of drag coefficient. A parametric study on amplitude at forcing frequency ratio of 2 showed a clear transition between two- and three-dimensional flows.

The studies by Poncet (2002, 2004) were confined near the cylinder ($5D$ to $6D$ from the cylinder location) and the parameter space was very limited. For example, it was only shown that at $F_R = 2$ beyond an oscillation amplitude of $\sim\pi/4$ two-dimensionality results but does the flow remain two-dimensional at all subsequent higher amplitudes or is there another bifurcation leading to three-dimensional effects? Jacono *et al.* (2010) have shown computationally at $Re = 300$ that at higher oscillation amplitudes after the suppression of mode A and B instabilities, a new mode (named as mode D), develops which can render the flow three-dimensional. Hourigan *et al.* (2007) have shown that the sequence of development of three-dimensional modes in bluff body wakes can be different depending on the shape and forcing conditions. This can have implications in the route to turbulence in such wake flows. The question of what happens in the far wake and at other forcing parameters is still open. These questions become important as new instability modes can develop as the wake evolves spatially (Thiria & Wesfreid 2007). In addition, there is lack of experimental evidence of any kind to show these effects. Three-dimensional aspects in combined translational and rotational oscillation of a cylinder in a quiescent fluid were studied by Nazarinia *et al.* (2009).

https://doi.org/10.1017/jfm.2013.469 Published online by Cambridge University Press

The present experimental study consists of studying the problem of flow past a cylinder executing rotational oscillations about its own axis for a wide range of amplitudes and forcing frequencies. The Reynolds number is fixed at 185; however, some studies are also conducted at *Re* of 400. It was realized after examining the existing literature that there are several questions which have either not been asked or only partially answered for this problem. Some of them are as follows. (i) What does the lock-on diagram look like in the forcing amplitude/frequency plane for wide range of forcing amplitudes? (ii) How does the lock-on diagram evolve with downstream distance from the cylinder? (iii) How does the frequency content of the wake evolve with downstream distance and how does it depend on forcing parameters? (iv) How does the far-wake frequency content change with forcing parameters? (v) Does the flow become more two-dimensional in the lock-in region? (vi) Does the change of mode shape at certain forcing parameters lead to wake becoming highly three-dimensional in a plane? (vii) Can the flow be made nominally two-dimensional in the far-wake even at moderately high *Re* of 400 and how does this control depend on forcing parameters? Keeping these questions in mind, the present comprehensive study was conducted. The answers to these questions will help provide some physical insight into the spatial evolution of bluff body wakes under forcing. More specifically, it will provide insight into stability characteristics: the evolution of new global modes in both two and three dimensions. This will help address some of the fundamental issues of bluff body wakes such as trends in the evolution of absolutely unstable and convectively unstable wake regions under forcing, return to global stability, stability characteristics of finite core vortex streets under forcing, spatial evolution (development/suppression) of three-dimensional modes which eventually determine the route the flow takes to become turbulent.

The cylinder was forced to oscillate according to

$$\theta = \theta_0 \sin(2\pi f t) \tag{1.1}$$

where θ is the angular position of the cylinder, θ_0 is the oscillation amplitude, f is the forcing frequency and t is time. The velocity amplitude, A, used by some researchers (such as Thiria *et al.* 2006) is related to the oscillation amplitude used in the present paper by the following relation

$$A = (D\pi f \theta_0)/U_\infty. \tag{1.2}$$

The vortex-shedding frequency from the stationary cylinder is denoted by f_0. The frequencies in the present paper are all non-dimensionalized using f_0. The ratio f/f_0 is called the frequency ratio and is denoted by F_R. The schematic of the problem investigated is shown in figure 1.

2. Experimental set-up and diagnostics

The experiments for the present study were carried out in a water tunnel (Rolling Hills Inc.: model 0710) with a test section of depth 0.25 m, length 0.46 m and width 0.18 m. The tunnel has a return circuit to recirculate the water using a 1.5 hp variable speed centrifugal pump. The sides of the test section are made of 6 mm thick tempered glass. The maximum speed of the flow can be 0.13 m s^{-1} and the turbulence intensity is less than 0.5 % root mean square (r.m.s.) at the experimental conditions. The water velocity needed to achieve $Re = 185$ was $\sim$0.03 m s^{-1} in the present experiments and was found to be uniform within 3.3 % in the middle 0.15 m width and 0.22 m depth of the test section before the effect of sidewall boundary layers can

https://doi.org/10.1017/jfm.2013.469 Published online by Cambridge University Press

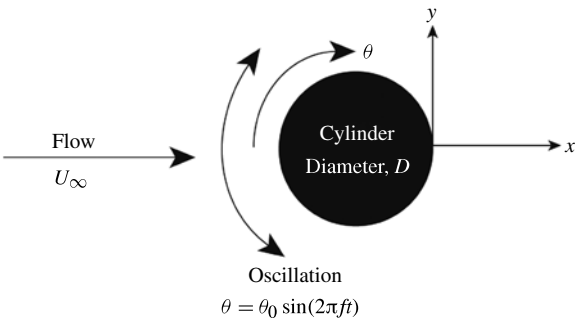


FIGURE 1. Schematic of the problem.

be felt. The flow uniformity was checked both by using the hot-wire anemometry and the PIV. The top of the tunnel test section is open and hence a rectangular piece of glass of size 475 mm × 184 mm × 3 mm, with a wide slot in the middle, was placed on top of the test section. During the experiments, the water surface was touching the glass. The cylinder was directly connected to a stepper motor and inserted from above midway between the two tunnel sidewalls through the slot in the glass cover. It spanned the full depth of the tunnel. The tunnel floor was a black anodized aluminum plate with a bearing in it to hold the cylinder. The bearing at the tunnel floor was housed in a streamlined housing with maximum thickness of 5 mm and streamwise extent of 50 mm. The experimental setup is schematically shown in figure 2.

The cylinder used in the experiments was a stainless steel rod of length 457 mm and diameter 6.35 mm. The cylinder had an aspect ratio of 39 based on the wetted length. The blockage resulting from the cylinder in the tunnel test section was 3.5 %. The cylinder was imparted sinusoidal rotary oscillations at various amplitudes and frequencies using a stepper motor (model: STM 23Q-3AE from applied motion products). The motor was computer controlled using the motor software (Q-programmer). The oscillation amplitude was controlled through this software. In addition, the motor was also coupled to a signal generator (model: HP 33120 A) which provided analogue sinusoidal signals of known frequency. This signal controlled the oscillation frequency of the cylinder.

The flow visualization was done using the hydrogen bubble technique. This was implemented with a 25 μm diameter platinum wire, acting as cathode, stretched across the width of the test section 5 mm upstream of the cylinder, and a small graphite plate, acting as anode, placed 406 mm downstream from the platinum wire. Potential difference of ∼12–18 V was sufficient to obtain good quality hydrogen bubbles in the present experiments. A small amount (∼40 g) of sodium sulfate was added to the water in the tunnel to facilitate the electrolysis and, hence, improve the bubble quality. The hydrogen bubbles formed on the platinum wire are swept downstream by the flow to form a sheet of bubbles. The bubble sheet was illuminated from the side by an overhead projector (model 3M-9100). The flow structures, made visible by the illuminated bubble sheet, were captured with a Sony HDR-HC5 digital video recorder mounted on a traverse mechanism and viewing perpendicular to the illumination and flow direction. The framing rate of the video camera provided sufficient resolution to characterize the flow features at relatively low Reynolds numbers of 185 and 400 in the present experiments. The end-view looking upstream (see figure 2) was captured with a still image CCD camera (model: Apogee U260, CCD 512 × 512 pixel). At high

https://doi.org/10.1017/jfm.2013.469 Published online by Cambridge University Press

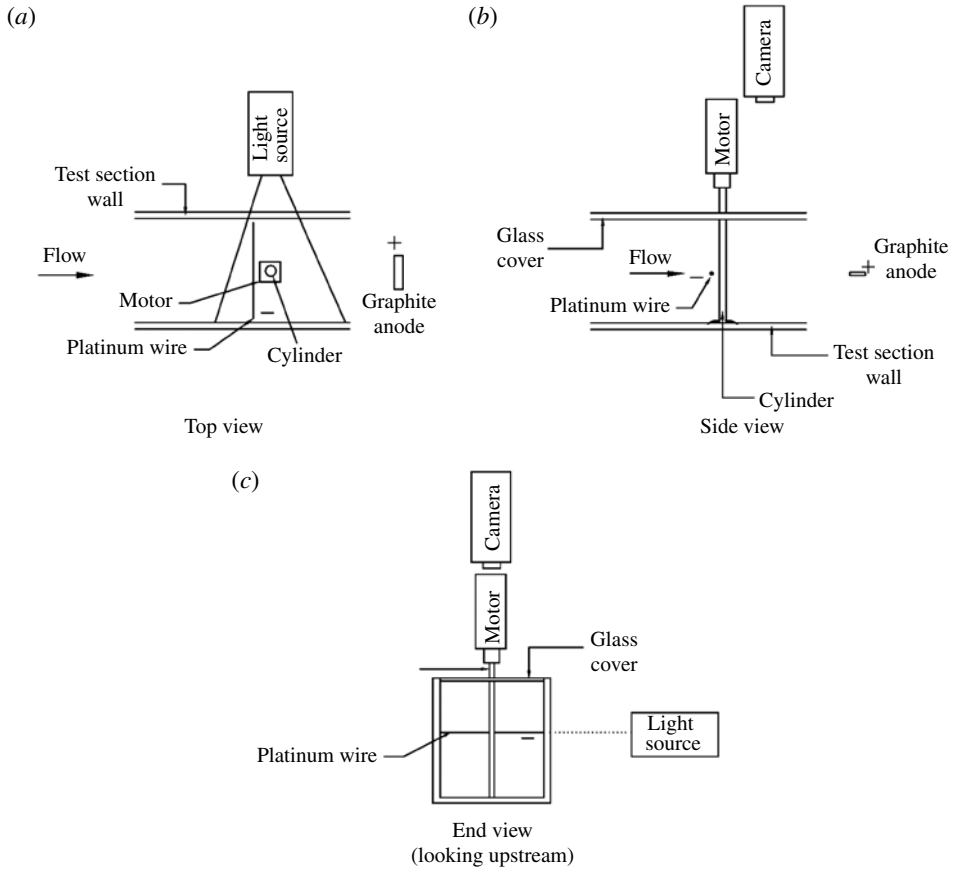


FIGURE 2. Schematic of the experimental set-up for flow visualization and PIV experiments: (*a*) top view; (*b*) side view; (*c*) end view (looking upstream). The platinum wire and graphite anode were absent for PIV studies.

oscillation amplitudes and frequencies ($\theta_0 \geqslant \pi/2$ and $F_R \geqslant 4.0$) a very small amount ($\sim\leqslant 0.1$ mm or $0.015D$) of lateral motion was observed in the visualization plane due to some clearance between the cylinder and the bearing for the rotation to take place smoothly.

The frequency content of the wake of the oscillating cylinder was measured by implementing hot-wire anemometry using a single sensor fibre-film probe. A Mini CTA system (model: 54T30) from Dantec Dynamics using a fibre film probe (model: 55R11) was used to acquire velocity fluctuation data. The probe was mounted on a straight holder and inserted from the downstream end of the tunnel. The sensor was placed at $y/D \sim 1.5$ for all the experiments. Data was acquired at 5 kHz for 15 s giving 75 000 samples for power spectrum calculations. Five downstream locations of $x/D = 2$, 4, 9 and 23 were used to study the evolution of wake spectral content at various forcing parameters.

The PIV measurements were done in the water tunnel in the same experimental conditions (but as different realizations) as the flow visualization experiments. The schematic of the PIV experiments is shown in figure 2 with the exception of the platinum wire and the graphite anode, which were absent. The light source and camera

https://doi.org/10.1017/jfm.2013.469 Published online by Cambridge University Press

were a laser and a PIV camera, respectively. A Dantec PIV system using Dynamic-Studio v 2.3 platform from Dantec was used to obtain quantitative information on the velocity and the vorticity fields. The system has been used in earlier studies of similar nature by the present authors (Kumar, Laughlin & Cantu 2009; Kumar, Gonzalez & Probst 2011*a*; Kumar, Cantu & Gonzalez 2011*b*) and has been tested to measure velocities with 2–3 % uncertainty. The flow was seeded with 10 μm diameter silver-coated hollow glass spheres and was illuminated in a horizontal plane just downstream of the cylinder with a laser sheet. The laser sheet was formed using the cylindrical lens optics in front of the New Wave laser (model: Solo PIV laser 120 XT, 15 Hz). The laser sheet was focused down to a thickness of less than 1 mm near the cylinder location. The digital images of the glass spheres (particles) in the plane of the laser sheet were captured using a HiSense-MkII CCD camera for PIV analysis. The size of the captured images was 1344 × 1024 pixels. The physical area covered by the images was 70 mm × 53 mm, corresponding to a magnification of ∼0.05 mm pixel^{-1}. The image processing was done using 32 × 32 rectangular interrogation areas with 50 % overlap in the horizontal and vertical directions. This resulted in the spatial resolution of 0.8 mm or 0.13D in the vorticity fields. The number of velocity vectors calculated in the imaged area were 83 × 63, i.e. 5229 vectors. The axial vorticity (component of vorticity along the cylinder axis), ω_z, was calculated from these velocity vectors at the same number of places.

The vortex-shedding frequency from the stationary cylinder, f_0, in the present experiments at $Re = 185$, was measured as 0.877 Hz. This gives a Strouhal number, St, defined as f_0D/U_∞, of 0.191 with an uncertainty of $\sim +/- 4$ %. In addition, for the stationary cylinder at $Re = 185$ the vortex shedding was observed to be slightly oblique (inclined at ∼5° with the cylinder axis) in a region of ∼20D around the visualization plane.

3. Results and discussions

The first part of this section discusses the flow visualization data at various forcing amplitudes and frequency ratios along with the spectral data. This is followed by geometrical analysis, PIV data and visualization study along the third dimension (end view). In the presentation of the results, the near field and far field are referred to as regions ∼0 to 17D and ∼20 to 35D, respectively, downstream of the cylinder.

3.1. *Planar flow visualization and spectral study*

Figure 3 shows the wake structure behind a cylinder executing rotary oscillations at amplitude of π/4 and various forcing frequencies. The downstream distance from the cylinder location visible in the images is ∼17D. The numbers on each frame represent non-dimensional forcing frequency, F_R. At low forcing frequency of 0.25 the vortex street is similar to a vortex street behind a stationary cylinder. The increase in forcing frequency results in distortion of the wake structure because of the nonlinear interactions between the forced frequency and the Strouhal frequency. This is seen in figure 3 for forcing frequencies of 0.5 and 0.7. The wake resembles the familiar vortex street from a stationary cylinder with well-formed vortices for $F_R = 0.8$ to 1.0. Between $F_R = 1.0$ and 1.2 the wake mode geometry undergoes change with increased separation between the two rows of same signed vortices. This wake mode undergoes a transitional change with increasing F_R until at higher forcing frequencies small-scale vortices are shed which merge in a distance of about ∼2D to form a vortex street similar to that behind a stationary cylinder. The merging position of the small-scale

https://doi.org/10.1017/jfm.2013.469 Published online by Cambridge University Press

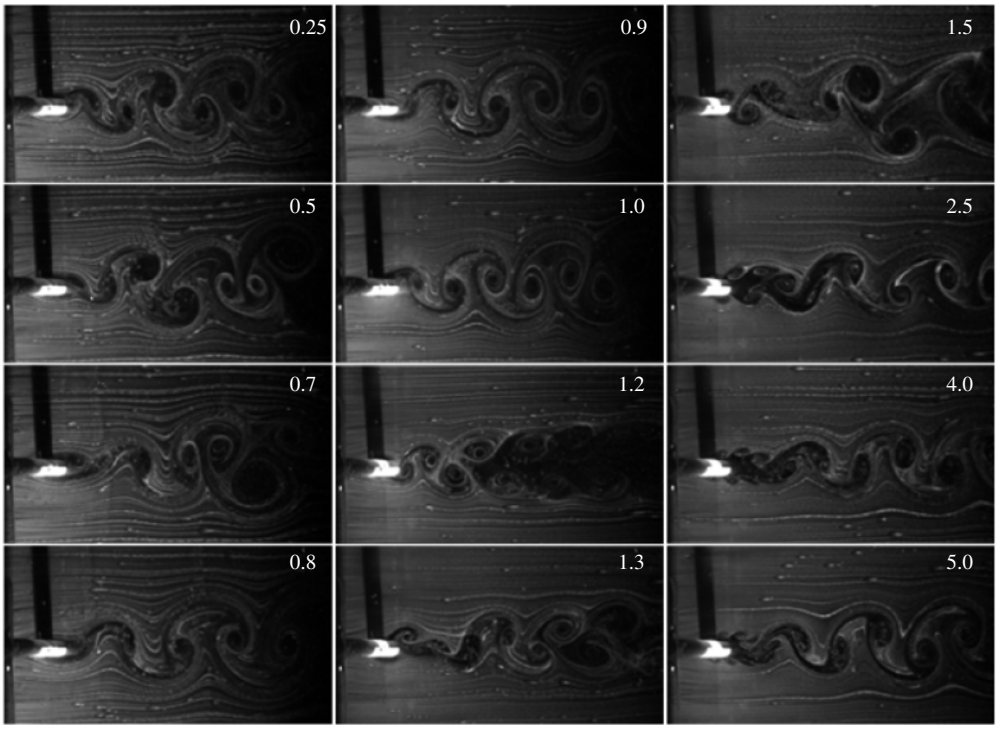


FIGURE 3. Wake structure for the forcing amplitude of $\pi/4$ between $x/D \sim 0$ and 17. The number on each frame represents the value of forcing frequency, F_R.

vortices comes closer to the cylinder as F_R is increased. This is seen from the wake structure at $F_R = 2.5$, 4.0 and 5.0 in figure 3.

The small-scale vortices that are shed at higher forcing frequencies at an oscillation amplitude of $\pi/4$ and higher (see, for example, figure 6 for oscillation amplitude of $\pi/2$ and figure 9 for oscillation amplitude of $3\pi/4$) appear in form to be very similar to the shear-layer vortices which are stimulated by very small rotational oscillations (oscillation amplitudes $\leqslant 5°$) as seen in the study of Filler, Marston & Mih (1991) and by very small-amplitude lateral oscillations (Chyu *et al.* 1995; Chyu & Rockwell 1996) near inherent frequency of the shear layer. Shear-layer vortices, in unforced cases, are not observed below $Re \approx 1100$ (e.g. Wei & Smith 1986). The small-scale vortices of the present experiments, which are locked on to the cylinder forcing frequency, should not be viewed as shear-layer vortices resulting from classical Kelvin–Helmholtz type of shear-layer instability because the perturbation amplitudes ranging from $\pi/8$ to π radians are not small and, in addition, the forcing frequencies are much higher than the inherent frequency of the shear layer, f_{SL}, which can be estimated from the relation suggested by Prasad & Williamson (1997), i.e.

$$f_{SL}/f_0 = 0.0235Re^{0.67}. \tag{3.1}$$

The development of the wake further downstream ($\sim 20D$ to $35D$) was studied by moving the hydrogen-bubble-producing wire further downstream. It has been shown by Cimbala, Nagib & Roshko (1988), using a smoke-wire technique in air, that the streakline images may give false information on vortical structures if viewed a

https://doi.org/10.1017/jfm.2013.469 Published online by Cambridge University Press

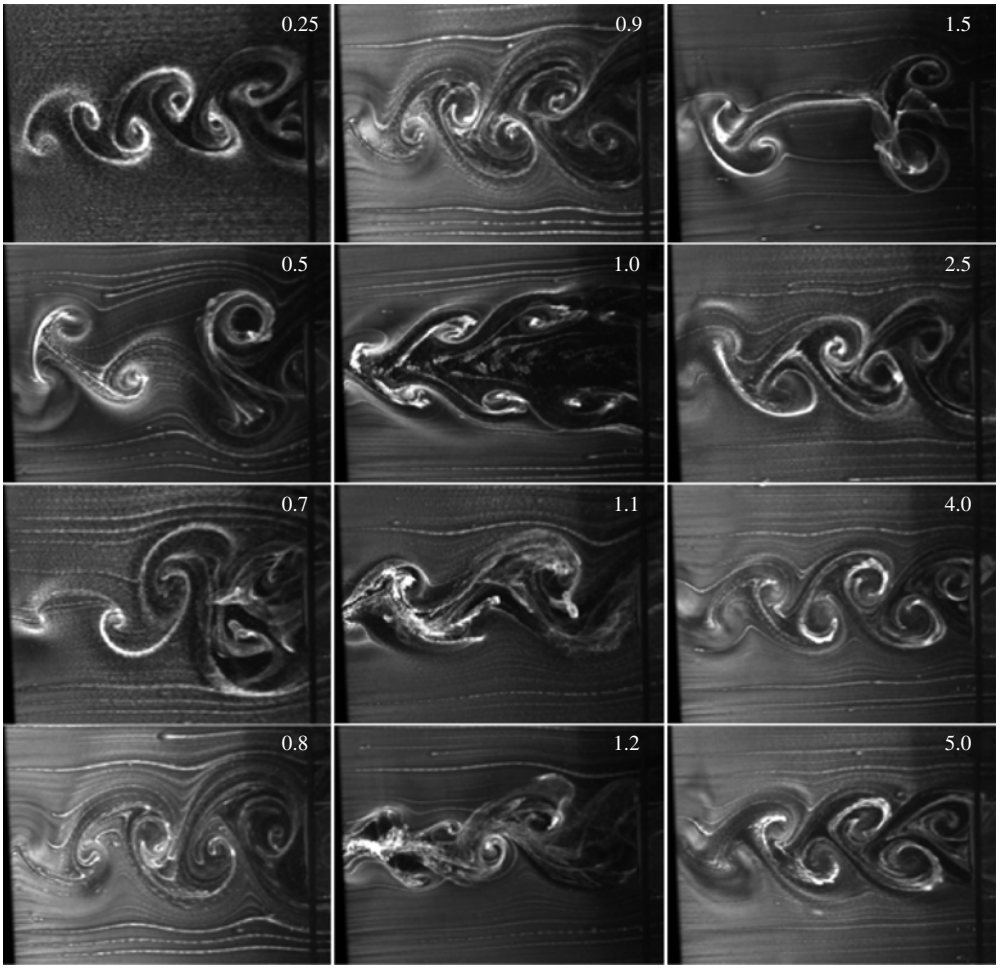


FIGURE 4. Wake structure for the forcing amplitude of $\pi/4$ between $x/D \sim 20$ and 35. The number on each frame represents the value of forcing frequency, F_R.

significant distance downstream ($\sim\geqslant 100D$ at present Re) due to mismatch of the dye and vorticity diffusion rates. However, in the present experiments, using hydrogen bubble technique, the downstream extent of flow visualization is only $\sim 15D$–$20D$ and the streaklines immediately after leaving the wire roll up giving a true picture of the vortical structures; hence, the issues addressed by Cimbala *et al.* (1988) are not applicable to the present case. The flow visualization results are shown in figure 4. The wake structure at low F_R of 0.25 shows a familiar vortex street with some modulation effect visible. The effects of multiple frequencies can be seen in the wake structures for forcing frequencies of 0.5 and 0.7 and the wake becomes very organized looking like a vortex street behind a stationary cylinder at F_R of 0.8 and 0.9. The wake mode changes between $F_R = 0.9$ and 1.0 with increased separation of the two rows of same-signed vortices. The wake structure at $F_R = 1.0$ is very different from the corresponding flow visualization image in figure 3. It seems that the wake undergoes through an instability between $x/D \sim 17D$ to $20D$ which results in vortices becoming flattened out and widely separated in the cross-flow direction. This wake

https://doi.org/10.1017/jfm.2013.469 Published online by Cambridge University Press

structure at $F_R = 1.0$ also goes through an instability resulting in large wavelength structures as is evident from the data at $F_R = 1.1$. The development of the far-wake structure with increasing forcing frequency presented here resembles the development of the far-wake structure for a stationary elliptical cylinder with increasing Reynolds number as presented by Hourigan *et al.* (2007). They showed the development of a secondary instability at downstream location resulting in the development of large-scale vortical structures from small-scale flattened out vortices similar to the present work. The transition to this secondary instability moved upstream with increasing Reynolds number. It appears to suggest that effect of increasing Reynolds number on the sequence of development of instabilities in the far wake for an elliptical cylinder is similar to the effect of increasing frequency in the present experiment. The wake structure of figure 4, after going through transitional change as forcing frequency increases, returns to the familiar vortex street structure behind a stationary cylinder at higher forcing frequencies as is clear from the data at $F_R = 2.5$, 4.0 and 5.0.

The frequency content of the wake is measured at four downstream distances, $x/D = 2$, 4, 9 and 23 with a single fibre-film probe using hot-wire anemometry. The results are shown in figure 5. The figure shows the development of the power spectrum of the streamwise velocity fluctuations with downstream distance at various values of forcing frequency, F_R. At low value of $F_R = 0.4$ the wake shows only Strouhal frequency for $x/D = 2$ to 9. The spectrum at $x/D = 23$ shows multiple peaks of approximately the same height showing that the wake in that region is in the phase of transition. The spectrum at $F_R = 0.6$ shows that the far wake at $x/D = 23$ has locked on to the forcing; however, the wake at $x/D = 0$ to 9 still is responding to the Strouhal frequency but there are clear indications of multiple frequencies present suggesting transitional complex behaviour. This transitional behaviour disappears and the wake shows a clear lock-on to the forcing at all distances from $F_R \sim 0.8$ to 1.0. This region also corresponds to a very well-defined Bénard–von Kármán vortex-street-like structure as shown in figure 3. The spectrum data shows that at $F_R = 1.1$, the spectrum at $x/D = 23$ separates from those at other distances where the wake is still locked on to the forcing and shows a much lower frequency which is approximately half that of the forcing. This is also seen in figure 4 that shows the change in wake mode with appearance of large wavelength structures. The lock-on at $x/D = 2$, 4 and 9 ends at $F_R = 1.4$ where the dominant frequencies at these locations returns to Strouhal frequency. An increase of forcing frequency reduces the near-wake region locked on to cylinder forcing to $\sim 1D$–$2D$ as F_R approaches 5.0 (see figure 3), the rest of the downstream wake decouples from the cylinder forcing frequency and starts behaving like the wake from a stationary cylinder with vortex-shedding frequency near the Strouhal frequency as shown by the behaviour of spectrum at $F_R = 4.0$ and 5.0. The spatial evolution of the wake described here can be seen in terms of change in the stability characteristics of the modified mean flow near the cylinder as discussed by Thiria & Wesfreid (2007) who show that the decoupled wake is a new global mode. The evolution of the spectrum in figure 5 shows that different regions of the wake can lock-on to the cylinder forcing in different forcing frequency range and display different structure.

The wake structure and its frequency content (not shown here) were also studied for a forcing amplitude of $\pi/8$. The near-field wake structure for a forcing amplitude of $\pi/8$ was observed to be very similar to the case for a forcing amplitude of $\pi/4$ shown in figure 3. The extent of the region adjacent to the cylinder, of small-scale vortices,

https://doi.org/10.1017/jfm.2013.469 Published online by Cambridge University Press

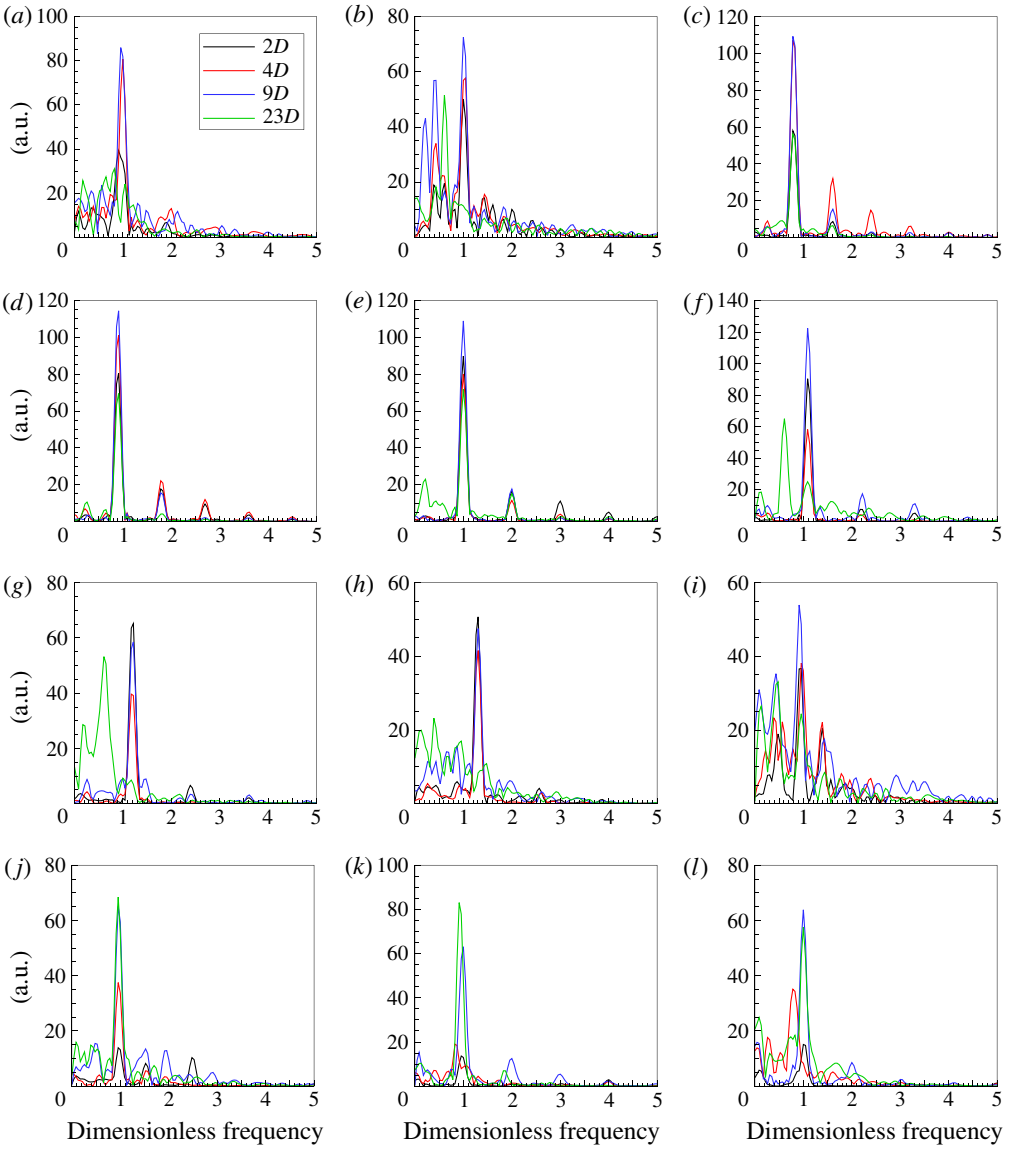


FIGURE 5. Spectrum evolution with the forcing frequency and downstream distance at a forcing amplitude of $\pi/4$: (*a*) $F_R = 0.4$; (*b*) $F_R = 0.6$; (*c*) $F_R = 0.8$; (*d*) $F_R = 0.9$; (*e*) $F_R = 1.0$; (*f*) $F_R = 1.1$; (*g*) $F_R = 1.2$; (*h*) $F_R = 1.3$; (*i*) $F_R = 1.4$; (*j*) $F_R = 2.5$; (*k*) $F_R = 4.0$; (*l*) $F_R = 5.0$.

at higher forcing frequencies near $F_R = 4.0$ and 5.0, was observed to be significantly smaller than the case for a forcing amplitude of $\pi/4$. The far-wake structure for a forcing amplitude of $\pi/8$ was also observed to be similar to the case of a forcing amplitude of $\pi/4$ shown in figure 4. The changes in mode shape that occurred between $F_R = 0.9$ and 1.0 and between $F_R = 1.0$ and 1.1 in figure 4 occurred between $F_R = 1.0$ and 1.1 and between $F_R = 1.1$ and 1.2, respectively, for a forcing amplitude of $\pi/8$. The lock-on region was from $F_R = 0.9$ to 1.2 at $x/D = 2$ to 9 and from $F_R = 0.7$ to 1.0 at $x/D = 23$.

https://doi.org/10.1017/jfm.2013.469 Published online by Cambridge University Press

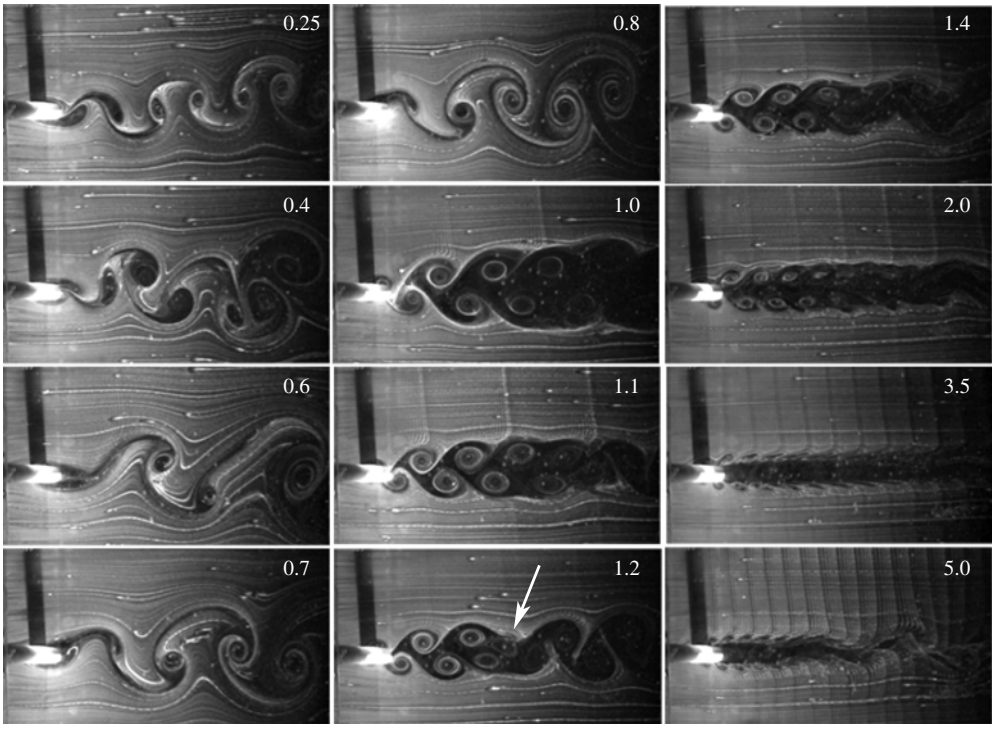


FIGURE 6. Wake structure for the forcing amplitude of $\pi/2$ between $x/D \sim 0$ and 17. The arrow in the frame at $F_R = 1.2$ shows an instance of vortex merger leading to mode shape change. The number on each frame represents the value of the forcing frequency, F_R.

Figures 6, 7 and 8 show, respectively, the near-field, the far-field and the spectrum content evolution with downstream distance when the amplitude of oscillation is $\pi/2$. The wake structure at $F_R = 0.25$ in the near field is similar to that behind a stationary cylinder with visible low-frequency modulation which is also evident in the far-field data at this forcing amplitude in figure 7 and in the supplementary movies, available online at http://dx.doi.org/10.1017/jfm.2013.469, at this setting. Increasing the forcing frequency changes the mode shape in the near wake, for example, using the nomenclature of Williamson & Roshko (1988), at $F_R = 0.4$ it resembles a P+S configuration which again changes to a 2S configuration at $F_R = 0.6$. The near-field wake structure at $F_R = 0.6$ shows long-wavelength structures suggesting locking on of the wake at this forcing. The vortex street in the near field at $F_R = 0.7$ and 0.8 exhibits well-formed vortical structures similar to regular vortex street behind a stationary cylinder and this continues even in the far field. Increasing the forcing to $F_R = 1.0$ causes a change in the mode shape which causes the vortex pair shed from the cylinder to have relatively larger inclination with respect to flow direction. This causes the two rows of vortices to have increased separation and appears as a distinct mode shape (double-row mode). This mode was also shown by Jacono *et al.* (2010) to be susceptible to newly discovered three-dimensional mode (mode D). Comparison of the wake structure at $F_R = 0.8$ and $F_R = 1.0$ in figure 6 shows that the first vortex formation occurs very close to the cylinder at $F_R = 1.0$ suggesting increased vorticity concentration in proximity of the cylinder at $F_R \sim 1.0$. Gu, Chyu & Rockwell (1994),

https://doi.org/10.1017/jfm.2013.469 Published online by Cambridge University Press

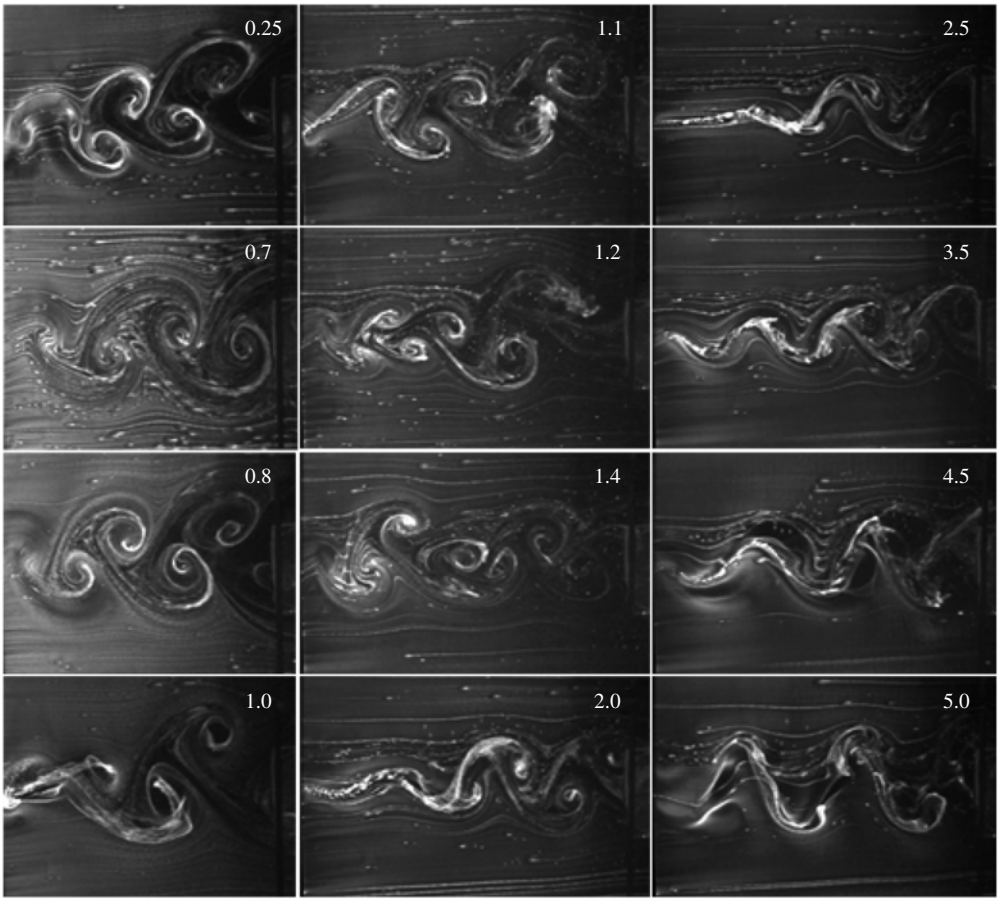


FIGURE 7. Wake structure for the forcing amplitude of $\pi/2$ between $x/D \sim 20$ and 35. The number on each frame represents the value of forcing frequency, F_R.

studying the effect of small lateral oscillations at $Re = 185$, observed abrupt changes in the streamline pattern and vorticity configuration near the cylinder at $F_R \sim 1.0$. They attributed this abrupt change to the vorticity concentration moving closer to the cylinder until a limiting position was reached. Possibly, a similar mechanism is responsible for change in mode shape at $F_R \sim 1.0$ observed in the present experiments.

The separation between the two rows of vortices decreases with further increase in forcing frequency as visible in the near-field wake structures in figure 6 resulting in a narrow wake. The size of the shed vortices also keeps decreasing with forcing frequency and they become more flattened. Similar phenomena of narrowing and widening wake widths, in the context of oscillating two-dimensional bodies immersed in potential flow, was theoretically studied by Weihs (1972) using semi-infinite rows of idealized point vortices. He established criteria when the vortex street would narrow, widen or remain of constant width and therefore provided some physical insight into the configurations of vortices in the forced vortex street case. Sometimes vertical lines are visible in the flow visualization frames of figure 6 at higher values of F_R, this is because the frame holding the hydrogen bubble wire was sometimes touching the motor frame which resulted, in some cases, in small vibration of the hydrogen-

https://doi.org/10.1017/jfm.2013.469 Published online by Cambridge University Press

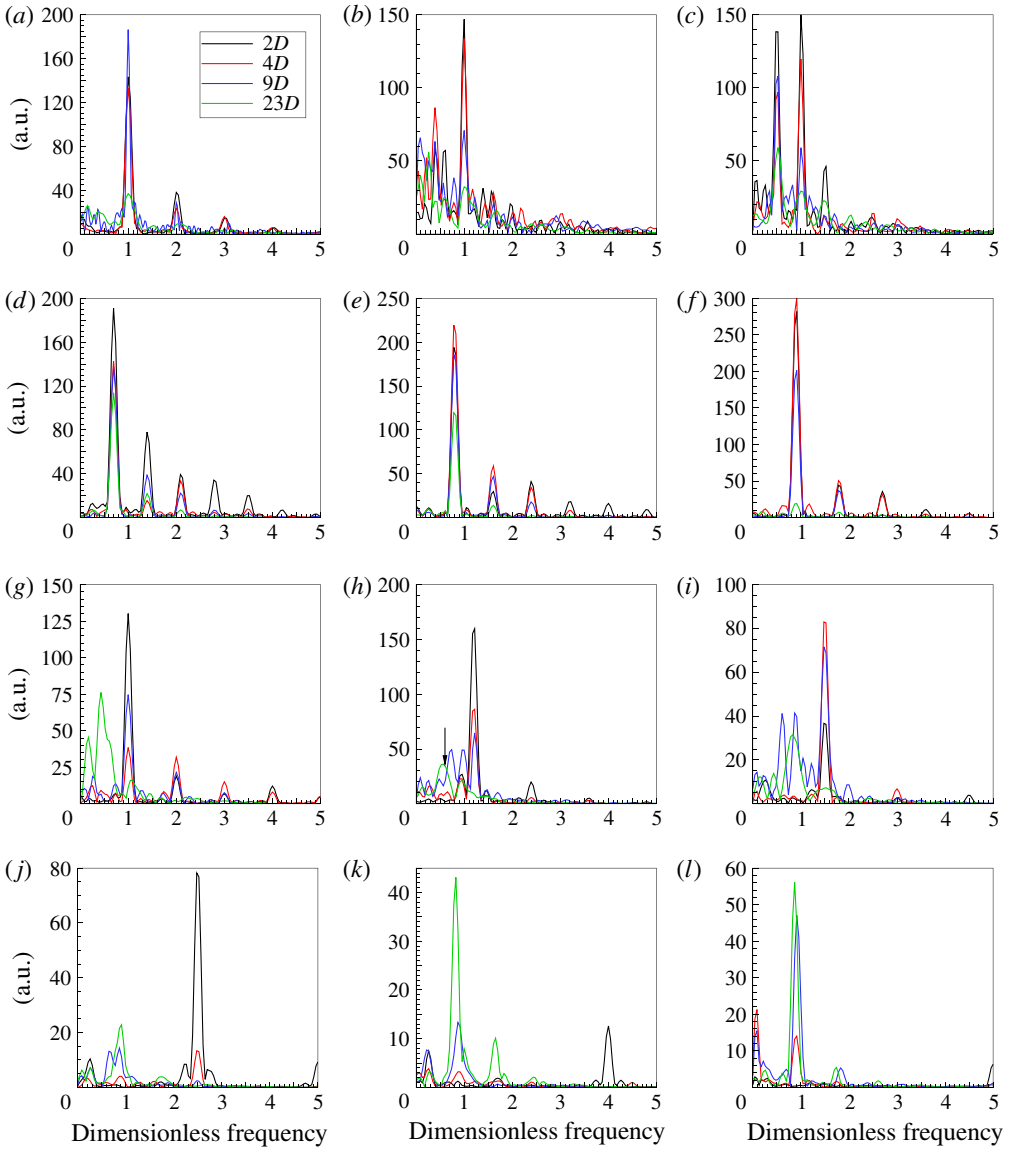


FIGURE 8. Spectrum evolution with forcing frequency and downstream distance at a forcing amplitude of $\pi/2$. The arrow in the spectrum for $F_R = 1.2$ at $x/D = 23$ shows an instance of subharmonic wake response at half the forcing frequency: (*a*) $F_R = 0$; (*b*) $F_R = 0.4$; (*c*) $F_R = 0.5$; (*d*) $F_R = 0.7$; (*e*) $F_R = 0.8$; (*f*) $F_R = 0.9$; (*g*) $F_R = 1.0$; (*h*) $F_R = 1.2$; (*i*) $F_R = 1.5$; (*j*) $F_R = 2.5$; (*k*) $F_R = 4.0$; (*l*) $F_R = 5.0$.

bubble-producing wire. This has a negligible effect on the forced cylinder wake as the Reynolds number for the hydrogen-bubble-producing wire is <1.0.

The vortices shed from the cylinder at $F_R \geqslant 1.0$ in each of the two rows merge (coalesce) resulting in evolution of a new global mode in the far wake with a different frequency as shown in figure 7. This was demonstrated by Thiria & Wesfreid (2007) as resulting from altered stability characteristics of the near-wake mean flow field.

https://doi.org/10.1017/jfm.2013.469 Published online by Cambridge University Press

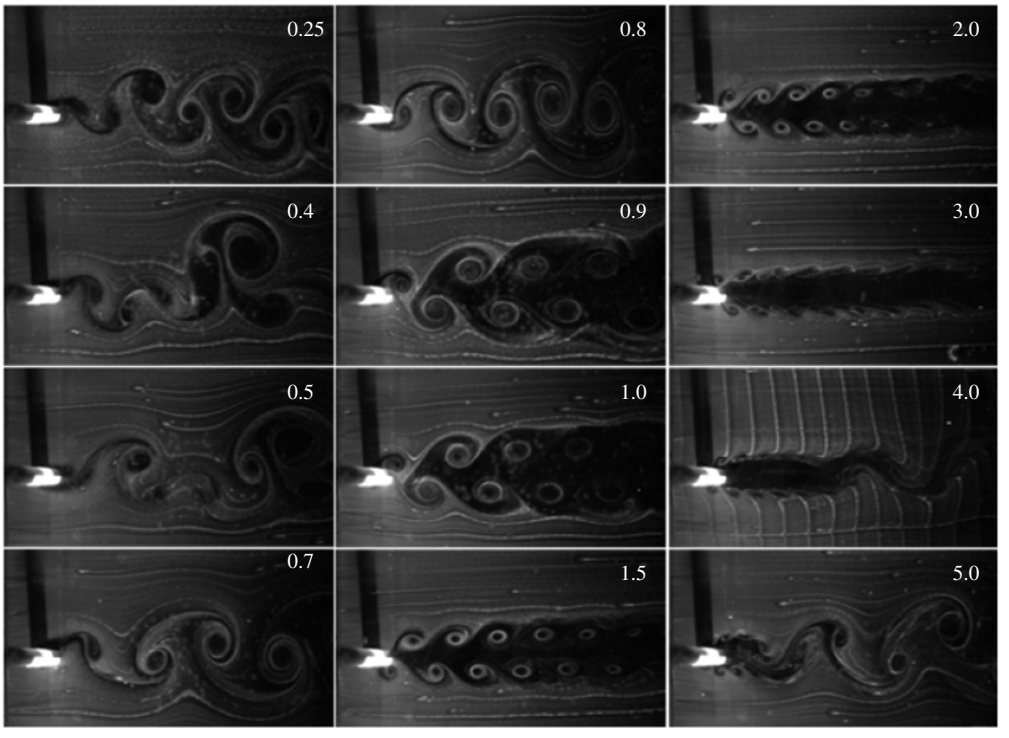


FIGURE 9. Wake structure for the forcing amplitude of $3\pi/4$ between $x/D \sim 0$ and 17. The number on each frame represents the value of forcing frequency, F_R.

This merging of vortices leading to the evolution of a new mode shape is clearly visible in the near-field wake structure at $F_R = 1.2$ in figure 6 (marked by an arrow) and in the online supplementary movies at this setting. This vortex-merging location moves upstream closer to the cylinder with increasing forcing frequency from $F_R = 1.0$ onwards. This is seen in figure 6 at $F_R = 1.0$ where only two rows of vortices are visible with no clear signs of merging in the limited viewing area to $F_R = 1.2$ where merging location is shown by an arrow. The merging location moved $\sim 2D$–$3D$ upstream as F_R increased from 1.1 to 1.2. Increasing F_R further causes the merging location to move downstream as seen at $F_R = 2.0$ where the merging location is almost out of the field of view. Further increase of F_R to higher values brings the merging location closer to the cylinder again as seen in $F_R = 5.0$ where merging occurs at $x/D \sim 8D$. This near-field wake structure at $F_R = 5.0$ is distinctly different from that corresponding to a lower amplitude of $\pi/4$ in figure 3 suggesting a strong effect of amplitude at this forcing frequency. The precise values of F_R at which the vortex-merger location changes its direction of motion was not investigated in the present work. The wake structure, in both the near and the far field, described here for a forcing amplitude of $\pi/2$ and various forcing frequencies can be seen in the online supplementary movies in a dynamic manner.

The spectrum of the streamwise velocity fluctuations at an oscillation amplitude of $\pi/2$ is shown in figure 8. The figure shows the spectrum evolution at various forcing frequencies with downstream distance. The figure also shows the no-oscillation case corresponding to $F_R = 0$ for comparison purposes where the wake has Strouhal

https://doi.org/10.1017/jfm.2013.469 Published online by Cambridge University Press

frequency at all measured downstream distances. The figure shows that locking of the wake to the forcing depends on the downstream location and the forcing frequency. In the forcing frequency range, $F_R = 0.7$ to 0.9, the wake is locked on to the forcing at all measured distances. The spectrum at $x/D = 23$ starts to separate from the spectra at $x/D = 2, 4$ and 9 at $F_R = 1.0$ suggesting the presence of a new global mode at this location with a lower dominant frequency. The lower dominant frequency or subharmonic observed at $x/D = 23$ is at half the forcing frequency, i.e. at 0.5. This is also consistent with the flow visualization data in figures 6 and 7 where the near and the far field show different wake structures resulting from change in mode shape due to vortex merger.

The spectrum at $F_R = 1.2$ and $x/D = 9$ shows multiple peaks, one at forcing and the other at lower frequencies, suggesting the initiation of the mode change process. This is also confirmed by the flow visualization data in figure 6 and in the online supplementary movies where the clearly visible vortex-merging process is occurring near $x/D = 9$ at $F_R = 1.2$. This vortex merger seen at $F_R = 1.2$ would produce a dominant subharmonic at half the forcing frequency due to period doubling immediately after $x/D \sim 9$. Since the newly evolved global mode shape does not change further downstream, the dominant frequency is expected to remain at half the forcing frequency and this is evident in the spectrum data for $F_R = 1.2$ at $x/D = 23$. This period doubling effect was also seen for $F_R = 1.0$ case. Increasing the forcing frequency causes the dominant frequency at $x/D = 23$ to come closer to the Strouhal frequency but is lower than the Strouhal frequency even at the highest forcing frequency. The spectra information also suggests that the dominant frequency of the wake comes closer to the Strouhal frequency (actually somewhat lower) as the forcing is increased at distances $x/D = 4$ and 9. The spectra close to the cylinder at $x/D = 2.0$ shows a dominant peak at the forcing frequency even for the highest forcing frequencies studied here which suggests that the very small vortices which are shed from the cylinder at higher values of forcing frequency as shown in figure 6 are shed at the forcing frequency and then they merge to evolve into a low-frequency wake. The spectrum showed peaks at lower frequencies at some forcing parameters such as at $F_R = 2.5$, 4.0 and 5.0. Such low-frequency modulation effects were also seen in the two-dimensional numerical simulations of Choi *et al.* (2002) who showed that the modulation effect was related to the vortex-merging process in the wake.

The increase of forcing oscillation amplitude to $3\pi/4$ and π qualitatively resulted in the wake behaviour similar to those described above for the oscillation amplitude of $\pi/2$ both in the near and far field. Figures 9 and 10 show, respectively, the near-field and the far-field wake structure for a forcing amplitude of $3\pi/4$. A very similar sequence of wake development with forcing frequency (not shown) was observed for a forcing amplitude of π. The combination of small-scale shed vortices at higher forcing frequencies to form larger vortex pairs occurred closer to the cylinder as compared with the wake dynamics at forcing amplitude of $3\pi/4$.

The spectrum evolution for forcing amplitudes of $3\pi/4$ and π are shown in figures 11 and 12. The far-wake spectrum at $x/D = 23$ starts to separate from the spectra at other downstream locations at a forcing frequency of $F_R = 0.9$ for a forcing amplitude of $3\pi/4$ and at $F_R = 0.8$ for forcing a amplitude of π. These are the forcing frequencies near which the near-field wake structure undergoes a change in mode shape with increased separation in two rows of shed vortices as can be seen from figure 9 for forcing amplitude of $3\pi/4$. This near-wake mode, whose vortices are locked on to the cylinder forcing frequency, evolves into new mode in the far wake by vortex pairing resulting in dominant subharmonic of half the primary frequency (period

https://doi.org/10.1017/jfm.2013.469 Published online by Cambridge University Press

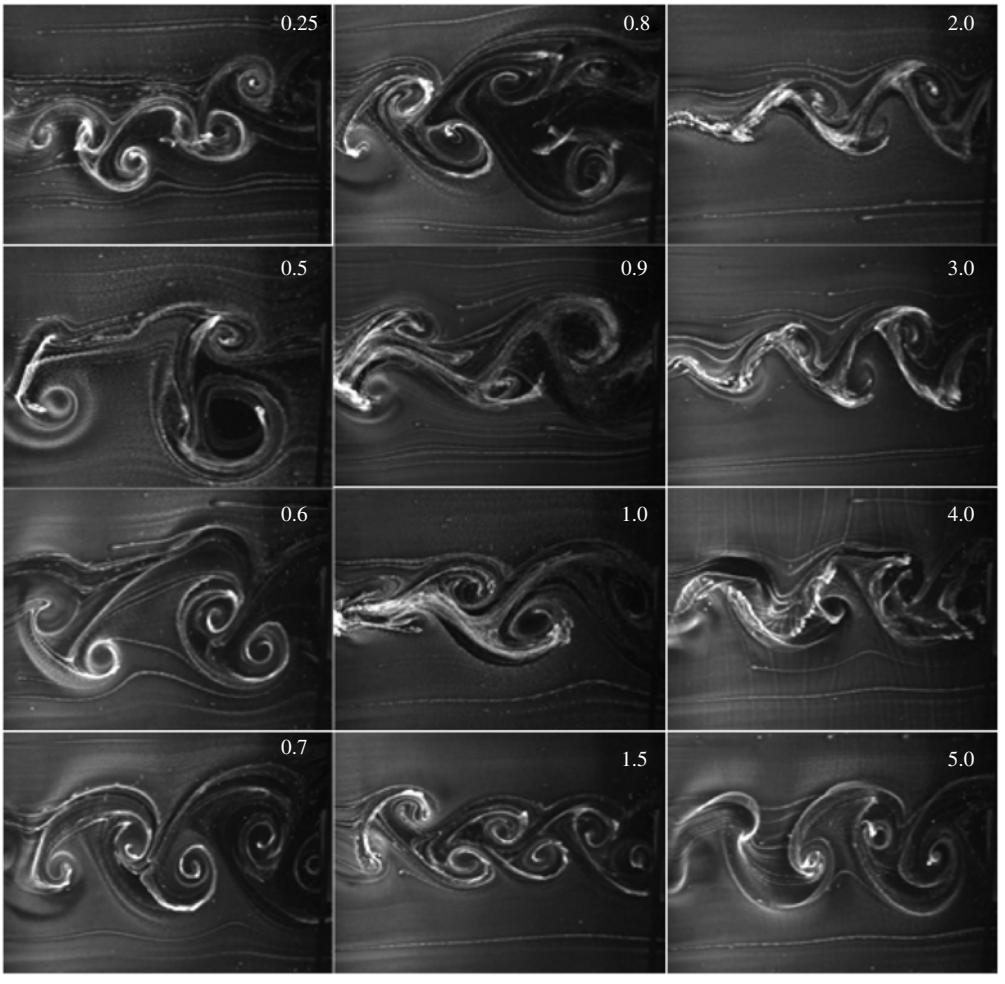


FIGURE 10. Wake structure for the forcing amplitude of $3\pi/4$ between $x/D \sim 20$ and 35. The number on each frame represents the value of forcing frequency, F_R.

doubling). This is seen in the spectrum of figure 11 at $x/D = 23$ for $F_R = 0.9$ and 1.0. Similar features are also seen in the spectrum study at forcing amplitude of π in figure 12 (for example, see spectrum at $F_R = 1.2$).

The behaviour of the spectrum in figure 11 for a forcing amplitude of $3\pi/4$ shows that the far-wake dominant frequency at $x/D = 23$ approaches the Strouhal frequency as the forcing frequency is increased and in fact shows a frequency somewhat higher than the Strouhal frequency (see the spectrum at $F_R = 4.5$). At other downstream distances and highest forcing frequencies, the dominant frequency is somewhat lower than the Strouhal frequency. The far-wake spectrum behaviour for a forcing amplitude of π in figure 12 shows that at higher forcing frequencies the dominant frequency is always lower than the Strouhal frequency (see, for example, the spectrum at $F_R = 4.5$ and 5.0 in figure 12). The lock-on regions are also clear in the spectrum plots. Thiria & Wesfreid (2007) were the first to have predicted the phenomenon of a far wake exhibiting lower than Strouhal frequency using linear stability analysis applied

https://doi.org/10.1017/jfm.2013.469 Published online by Cambridge University Press

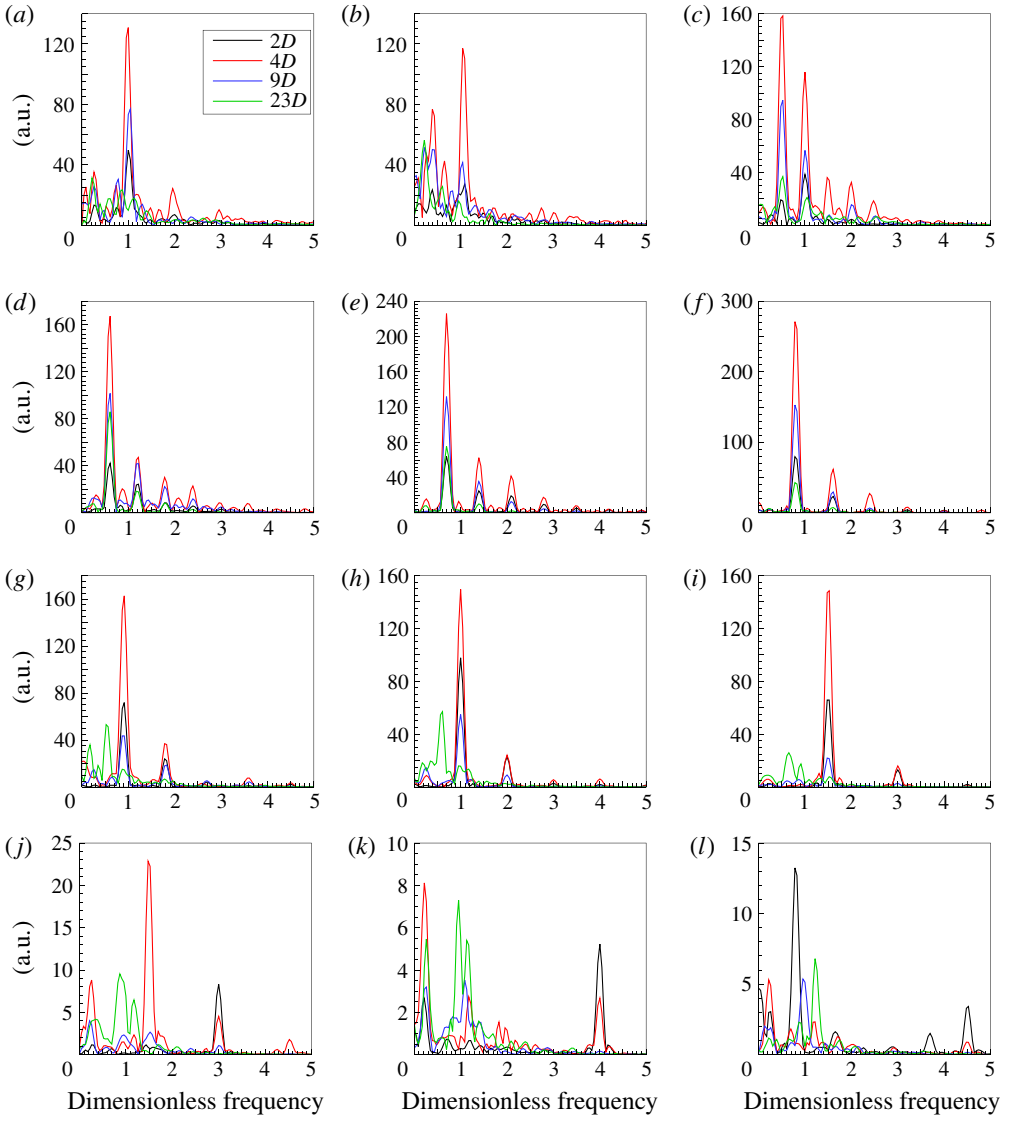


FIGURE 11. Spectrum evolution with the forcing frequency and downstream distance at a forcing amplitude of $3\pi/4$: (*a*) $F_R = 0.25$; (*b*) $F_R = 0.4$; (*c*) $F_R = 0.5$; (*d*) $F_R = 0.6$; (*e*) $F_R = 0.7$; (*f*) $F_R = 0.8$; (*g*) $F_R = 0.9$; (*h*) $F_R = 1.0$; (*i*) $F_R = 1.5$; (*j*) $F_R = 3.0$; (*k*) $F_R = 4.0$; (*l*) $F_R = 4.5$.

to averaged mean flow. They showed experimentally and theoretically using linear saddle-point criterion, specifically for $F_R = 5.0$ and velocity amplitude, $A = 5$, that the wake supports a new global mode with global frequency $\sim$85 % of the Strouhal frequency. The present experiments are in accordance with those predictions except at the forcing amplitude of $3\pi/4$ where the present experiments report higher than Strouhal frequency at higher forcing frequencies. The spectrum at forcing amplitude of $3\pi/4$ in figure 11, for instance, suggests that the wake at $F_R = 0.5$ to 0.8 does not support a new global mode because the dominant frequency is just the forcing frequency at all downstream locations. Wakes in such forcing conditions are

https://doi.org/10.1017/jfm.2013.469 Published online by Cambridge University Press

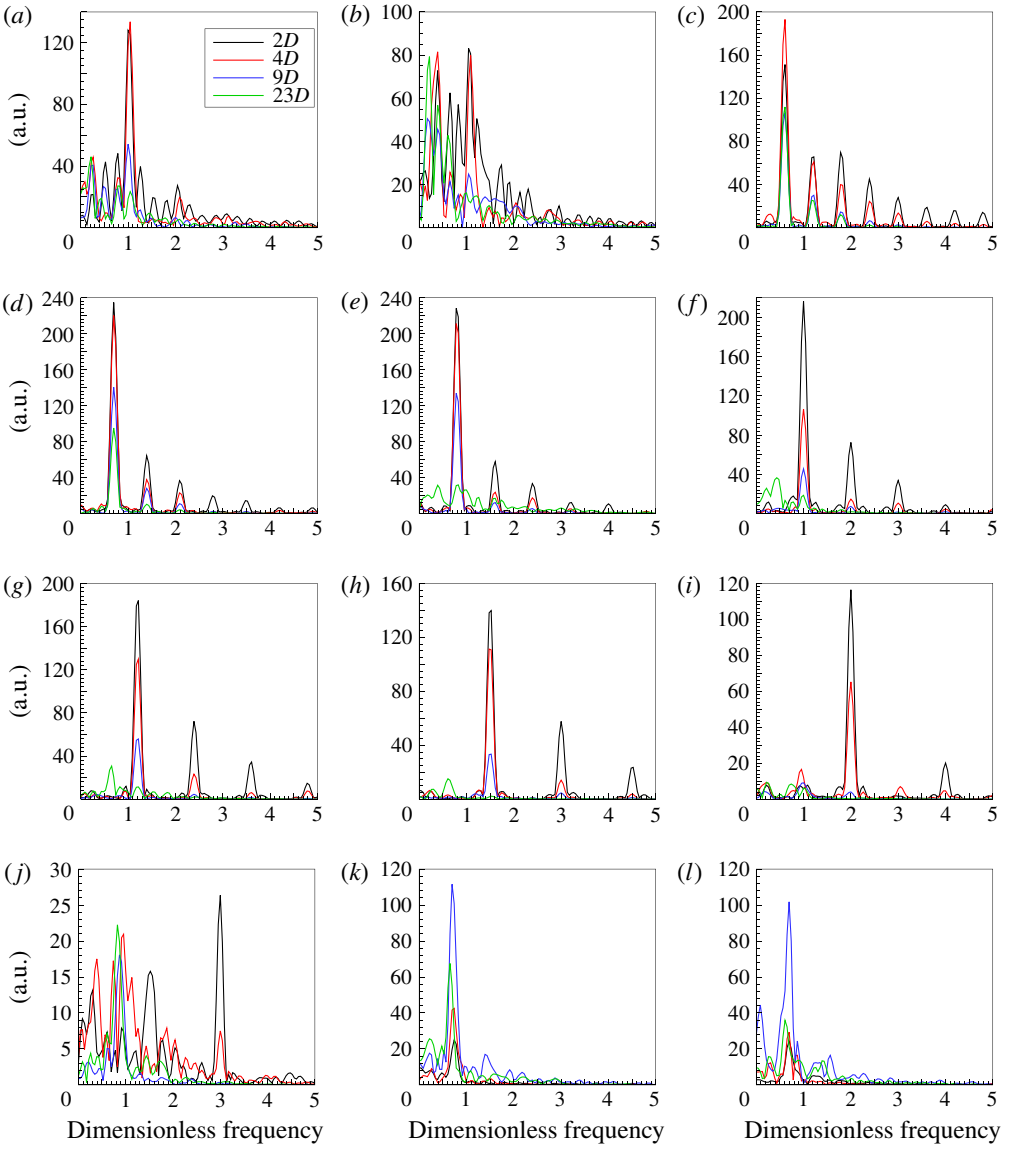


FIGURE 12. Spectrum evolution with the forcing frequency and downstream distance at a forcing amplitude of π: (*a*) $F_R = 0.25$; (*b*) $F_R = 0.4$; (*c*) $F_R = 0.6$; (*d*) $F_R = 0.7$; (*e*) $F_R = 0.8$; (*f*) $F_R = 1.0$; (*g*) $F_R = 1.2$; (*h*) $F_R = 1.5$; (*i*) $F_R = 2.0$; (*j*) $F_R = 3.0$; (*k*) $F_R = 4.5$; (*l*) $F_R = 5.0$.

convectively unstable throughout with vanishing absolutely unstable region near the cylinder (Thiria & Wesfreid 2007). Interestingly, as shown later in figure 23, this is also the region where the wake three-dimensionalities appear to be suppressed suggesting a connection between vanishing of absolutely unstable region due to surface forcing near the cylinder to suppression of three-dimensional flow.

Figure 13 shows the evolution of the far-wake vortex-shedding frequency at $x/D = 23$ for various forcing frequencies and forcing amplitudes after the lock-on phase at this downstream location. The figure also shows that the shedding frequency can be as low as ∼50 % of the Strouhal frequency, depending on the forcing

https://doi.org/10.1017/jfm.2013.469 Published online by Cambridge University Press

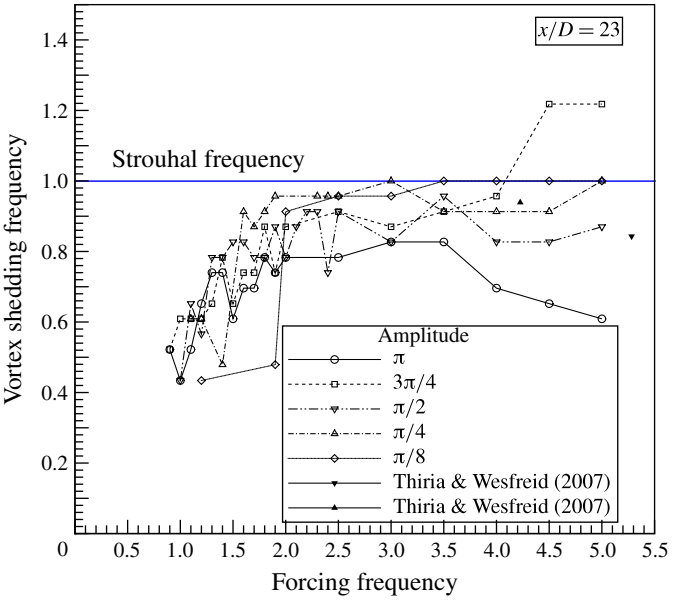


FIGURE 13. (Colour online) Vortex-shedding frequency dependence on forcing frequency and amplitude after lock-on at $x/D = 23$. The data of Thiria & Wesfreid (2007) at $Re = 150$, shown by filled symbols, corresponds to the amplitudes of the present experiments, shown by the corresponding open symbols.

amplitude, immediately after lock-on again suggesting vortex pairing resulting in period doubling as a mechanism to generate a new global mode. Increasing the forcing frequency causes the shedding frequency to increase and then saturate to a level somewhat lower than the Strouhal frequency except for forcing amplitude of $3\pi/4$, as noted above, where the shedding frequency was observed to be ~20–25 % higher than the Strouhal frequency. The asymptotic value of the vortex-shedding frequency is closer to the Strouhal frequency for lower forcing amplitudes; in fact, at a forcing amplitude of $\pi/8$ the shedding frequency is the same as the Strouhal frequency beyond $F_R = 3.5$. At the highest forcing frequency of 5.0, the highest forcing amplitude of π resulted in a shedding frequency ~60 % of the Strouhal frequency and ~87 % of Strouhal frequency for a forcing amplitude of $\pi/2$. Vortex shedding at 90–95 % of the Strouhal frequency was observed at the forcing amplitude of $\pi/4$ beyond $F_R = 1.8$ and then matched the Strouhal frequency at $F_R = 5.0$. The data of Thiria & Wesfreid (2007) has also been plotted in figure 13 for higher frequencies at amplitudes of $\pi/4$ and $\pi/2$ of the present experiments showing good agreement.

The lock-on region was extracted from the spectrum of the streamwise velocity fluctuations at various forcing amplitudes studied in the present investigation. Figure 14 shows the lock-on region in the forcing amplitude–forcing frequency plane (θ_0–F_R plane). The figure shows for each forcing amplitude, at each downstream location, the lower and upper limits of the region of forcing frequencies in which the dominant wake frequency is the same as cylinder forcing frequency. It is clear from the figure that the lock-on region not only depends on the forcing amplitude but also on the downstream location from the cylinder. The reason for this is the variability in the downstream location where the starting of new global mode due to coalescence of the near-wake vortices occurs. This variability possibly occurs due to

https://doi.org/10.1017/jfm.2013.469 Published online by Cambridge University Press

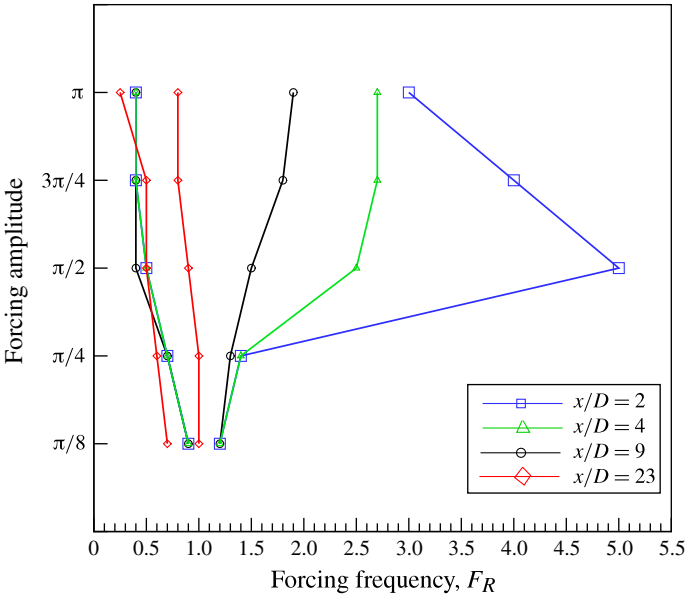


FIGURE 14. Lock-on diagram: regions showing lock-on in the forcing amplitude–forcing frequency plane at various downstream distances. The data points at five discrete amplitudes are joined by straight lines just to show the trend of the lock-on boundary.

changes in the mean flow stability characteristics near the cylinder (Thiria & Wesfreid 2007). At downstream distances of $x/D = 2$, 4 and 9, the lock-on region increases for forcing amplitudes ranging from $\pi/8$ to $\pi/2$ and thereafter shows a very slow increase or in some cases is almost stationary (see for $x/D = 4$ and 9). The region close to the cylinder near $x/D = 2$ shows a decrease in the lock-on region beyond a forcing amplitude of $\pi/2$. The lock-on regions at $x/D = 2$, 4 and 9 encompass the case of $F_R = 1$ for all forcing amplitudes. The lock-on region in the far field at $x/D = 23$ shows an interesting trend with the width of the lock-on region remaining almost constant for all forcing amplitudes; however, the region drifts towards the low-frequency side with increasing forcing amplitude. The case $F_R = 1$, in this case, is not encompassed in the lock-on region but is, at most, on the high-frequency boundary. Figure 14 also shows that the low-frequency boundaries of the lock-on regions for all forcing amplitudes are very close to each other for all downstream distances; however, the high-frequency boundaries show a strong dependence on the downstream location. It has been reported in the literature (Mahfouz & Badr 2000) that below a threshold value of forcing amplitude there is no lock-on, i.e. the lock-on region diminishes to zero; however, no such attempt was made in the present experiments to find this threshold value which probably is much lower than the lowest forcing amplitude studied in the present experiments.

The study of flow visualization data revealed that the near-field wake structure strongly depends on the forcing amplitude and forcing frequency. The distance between the vortices in the row of same-signed vortices and the distance between the two rows of vortices changes as the forcing amplitude and forcing frequency are varied. These distances can sometimes change suddenly when the mode shape changes at certain forcing parameter values, such as the change of mode shape at a forcing amplitude of $\pi/2$ between forcing frequencies of 0.8 and 1.0 in figure 6.

https://doi.org/10.1017/jfm.2013.469 Published online by Cambridge University Press

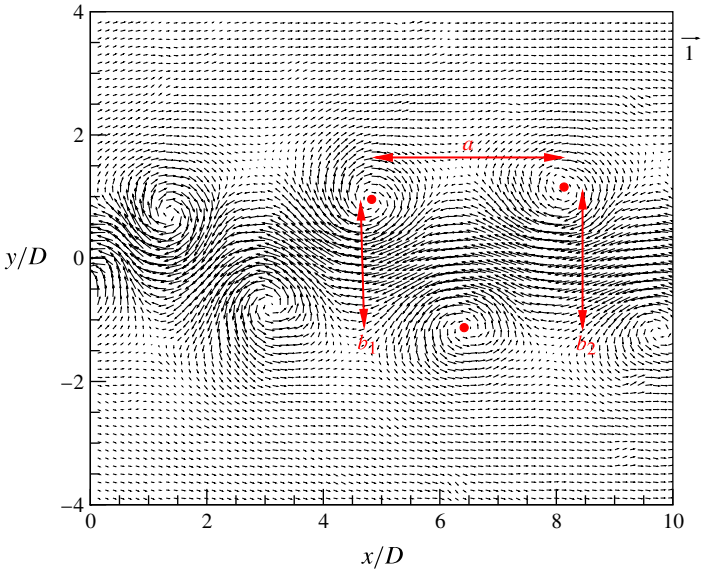


FIGURE 15. (Colour online) Illustration of the inter-vortex spacing measurement parameters for the case of forcing amplitude of $\pi/2$ and $F_R = 1.0$. The average of b_1 and b_2 is denoted by b.

The changes in the inter-vortex spacings with forcing parameters was studied in the present study in cases where the wake structure was stationary which included the lock-on region. The centres of the vortices were defined using the mean-subtracted velocity field data from PIV as shown in figure 15 for the case of $\theta_0 = \pi/2$ and $F_R = 1.0$ as an illustration. These measurements were taken between $x/D = 4$ and 9.0. The vortex spacing between two vortices in a row is denoted by a and the average spacing between the two rows of vortices is defined by $b = (b_1 + b_2)/2$. Figure 16 shows the effect of forcing parameters on a and b. Figure 16(a) shows that the inter-vortex spacing, a, in a row decreases as the forcing frequency is increased for all amplitudes. This spacing approaches the cylinder diameter, as the forcing frequency is increased, for forcing amplitudes of $\pi/2$, $3\pi/4$ and π and the range of forcing frequencies studied. A power-law curve of the form $a/D = 4.03F_R^{-1.06}$ to all of the data in figure 16(a) provides a good fit ($R^2 = 0.86$) showing that the inter-vortex spacing in a row and forcing frequency are almost inversely proportional to each other except for the lowest forcing frequencies.

Figure 16(b) shows the variation of b/a with forcing frequency for various forcing amplitudes. The ratio b/a shows an increasing trend with forcing frequency. The ratio shows a jump near $F_R \sim 1.0$ which corresponds to a change in mode shape with increased separation of two rows of vortices. This can be seen, as an example, from the flow visualization data in figure 9 which shows a change in mode shape from $F_R = 0.8$ to 0.9 and the corresponding variation of b/a in the figure 16(b) near this forcing frequency region. The forcing frequency at which the mode shape changes decreases as forcing amplitude is increased, ranging from $F_R \sim 1.2$ at $\theta_0 = \pi/8$ to $F_R \sim 0.8$ at $\theta_0 = \pi$. The ratio b/a of the two rows of vortices in a vortex street assumes importance from the stability characteristics point of view. The linear stability analysis of two rows of line vortices in both symmetric and staggered configuration was first carried out by Kármán (1911, 1912) who showed that only staggered

https://doi.org/10.1017/jfm.2013.469 Published online by Cambridge University Press

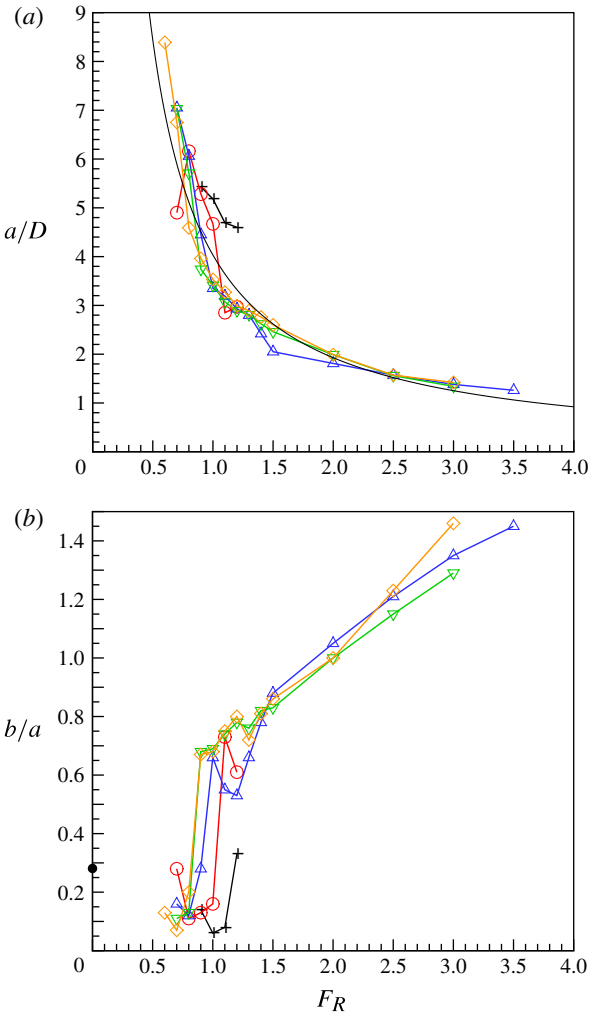


FIGURE 16. Geometry of the wake structure between $\sim x/D = 4$ and 9. (*a*) Variation of a/D with forcing frequency F_R and amplitude. The solid line is a power-law curve fit, $a/D = 4.03F_R^{-1.06}$, to all of the data. (*b*) Variation of b/a with forcing frequency F_R and amplitude. Symbols: $+$, $\theta_0 = \pi/8$; $\circ$, $\theta_0 = \pi/4$; $\triangle$, $\theta_0 = \pi/2$; ∇, $\theta_0 = 3\pi/4$; $\diamond$, $\theta_0 = \pi$; $\bullet$, stability ratio for an unforced vortex street of a cylinder wake modelled as line vortices according to Kármán (1911, 1912).

configuration was stable with b/a assuming a value of 0.281. Lamb (1932) gives a detailed derivation of this result. In the presence of forcing by rotational oscillations the present results show that this stability ratio can be stretched to $\sim$1.5 in the near-wake region.

3.2. *PIV results*

3.2.1. *Methodology*

PIV images were acquired at a rate four times the driving frequency for frequency ratios of 0.25 and 0.4–1.5 (steps of 0.1), as well as for 1.25. For F_R values ranging from 2.0 to 5.0 (steps of 0.5) the sampling frequency was twice the forcing frequency.

https://doi.org/10.1017/jfm.2013.469 Published online by Cambridge University Press

A total of 40 images were acquired for each setting; images corresponding to the same set of settings were phase-averaged after applying an image cross-correlation technique described below. While an optimal phase selection can in principle be achieved with a hardware-based trigger method based on an external reference, such as an appropriate pressure signal, such additional instrumentation can be avoided by image correlation techniques, e.g. as described by Konstantinidis, Balabani & Yianneskis (2005), Negri, Cozzi & Malavasi (2011), and others. Such techniques have been shown to be capable of achieving similar accuracies for quasi-periodic flows compared to hardware-based techniques, without requiring the experimental set-up used for methods with an external reference (Konstantinidis *et al.* 2005; Negri *et al.* 2011).

In order to ensure an optimal phase-averaging process, a comprehensive strategy was devised. The general approach is based on the idea of determining the optimal phase lag between an image of a series for a given parameter set (forcing amplitude and frequency, Reynolds number) and a suitable reference image of the same set, i.e. the phase lag leading to the maximal cross-correlation coefficient. A threshold value for the optimal correlation coefficient is required for an image to be included in the averaging of the series, thereby allowing to eliminate poor-quality images from the series which would otherwise contaminate the averaged result. In addition, a maximal value of the optimal lag between a given image and the reference image was allowed in order to avoid excessive image cropping. As the reference image for a given series is arbitrary, the optimal reference image for a given series is determined by the requirement that the average optimal correlation coefficient of the reference images with all other images in the series be maximal.

Once a phase-averaged PIV image for a given pair of driving frequency and amplitude had been produced, a threshold was applied to the image to detect either the area of positive or negative vorticity. In order to discriminate the vortices from the background noise a constant threshold value of ± 0.074 (in units of $U_\infty D$) was used. Since this procedure detects all vortices, as opposed to the first fully detached vortices to be analysed in this study, a decision had to be made as to the automatic versus semi-manual detection of the first detached vortex. While in the case of very stationary sequences automatic detection was found to be viable, semi-manual selection was found to be a safer strategy. For this procedure, an additional filter was applied, setting all images pixels of the prefiltered images outside of a predefined range to zero. Since the position of the first vortices is not stable, the filter bounds had to be adjusted manually for each frequency ratio and amplitude. Figure 17 shows typical phase-averaged vorticity fields for forcing amplitude of $3\pi/4$ and forcing frequency ratios of 0.8, 0.9 and 1.0.

3.2.2. *PIV data analysis results*

The circulation, Γ, of the first detached vortex was calculated in non-dimensional form defined as $\Gamma/U_\infty D$. The results are plotted in figure 18 against the forcing frequency ratio, F_R, for forcing amplitudes of $\pi/4$, $\pi/2$, $3\pi/4$ and π. An average of the absolute circulation values of the first detached positive and negative vortices was plotted in order to avoid cluttering of the figure. To a good approximation the absolute values of the positive and negative circulation values coincided in all cases. It is evident from figure 18 that circulation of the first detached vortex reaches a maximum value and then decreases with increased forcing frequency. The maximum of circulation is reached at $F_R = 1.0$ for forcing amplitude of $\pi/4$ and moves to lower values of F_R with increasing forcing amplitude reaching a value of ~ 0.7 for forcing

https://doi.org/10.1017/jfm.2013.469 Published online by Cambridge University Press

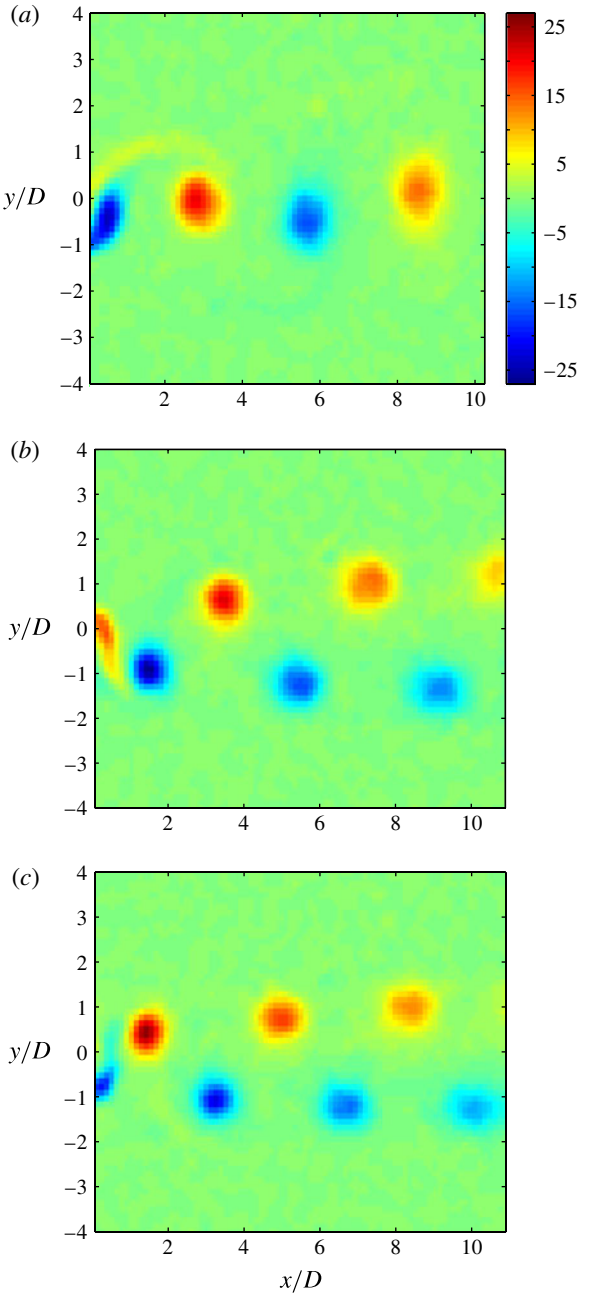


FIGURE 17. Phase-averaged vorticity field for a forcing amplitude of $3\pi/4$: (*a*) $F_R = 0.8$; (*b*) $F_R = 0.9$; (*c*) $F_R = 1.0$.

amplitude of π. For forcing frequencies, $F_R < 1$, a clear dependency of circulation on the forcing amplitude can be seen with circulation values increasing with forcing amplitude at a given forcing frequency.

In the present problem, the vorticity flux from the cylinder surface to the fluid occurs due to two reasons: the tangential surface acceleration and surface pressure

https://doi.org/10.1017/jfm.2013.469 Published online by Cambridge University Press

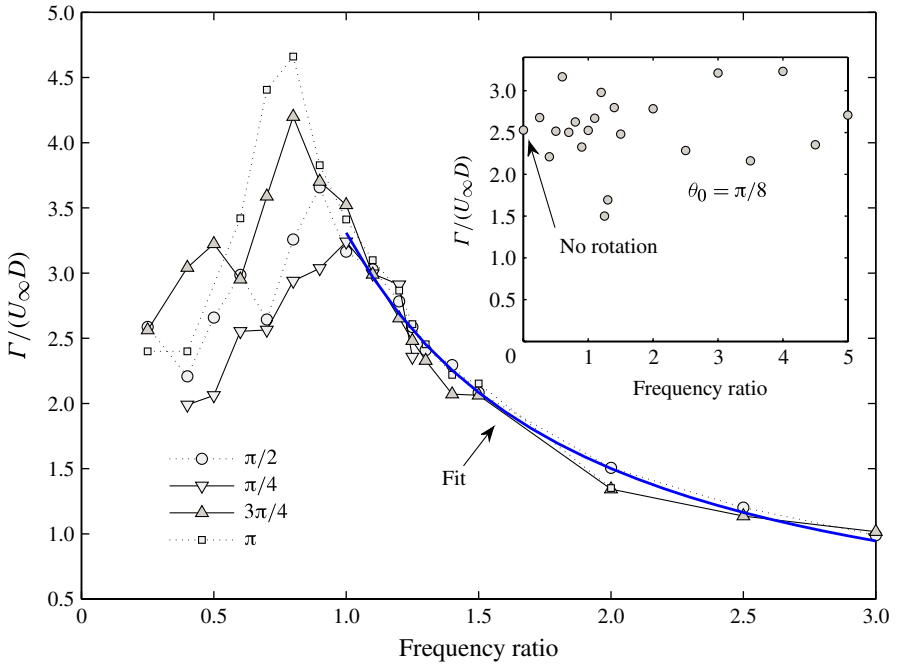


FIGURE 18. (Colour online) Variation of the normalized vortex circulation, $\Gamma/U_\infty D$, of the first detached vortex with forcing parameters.

gradient. The vorticity thus generated feeds into the evolving vortex. Thiria *et al.* (2006) showed that the phase relation between the cylinder motion direction and the evolving vortex determines whether the circulation of the shed vortex increases or decreases. They show that for $F_R \sim 1.0$ the circulation of the shed vortex peaks when the direction of cylinder motion is opposite to the direction of evolving vortex roll-up at the cylinder during the complete period of vortex formation (constructive interaction). This is also the value of F_R where the wake undergoes a change of mode shape from a convectively unstable wake with vanishing absolutely unstable region (complete lock-on at all downstream locations) to a double-row near wake which supports a new global mode (Thiria & Wesfreid 2007). The present experiments show that the circulation of the first shed vortex reaches maximum at such transition value of F_R at various oscillation amplitudes. At higher values of F_R, Thiria *et al.* (2006) showed that during the period of vortex formation near the cylinder there are times when the direction of cylinder motion and direction of vortex roll up are the same (destructive interaction) and this leads to a reduction in vortex circulation. At much higher frequencies they show that the cylinder motion direction and vortex roll-up direction are the same during the complete period of vortex formation. The present experiments, with similar wake morphologies, show such a decay in vortex strength with forcing frequency and in addition show that the circulation values seem to become almost independent of forcing amplitude beyond forcing frequency, $F_R = 1.0$. This is seen from the collapse of data in this range in figure 18 and circulation decay appears to follow a common decay curve. The physical basis for weak dependence of circulation on forcing amplitude beyond $F_R = 1.0$ possibly lies in the destructive interaction conditions that prevail in this range of forcing (Thiria *et al.* 2006). When

https://doi.org/10.1017/jfm.2013.469 Published online by Cambridge University Press

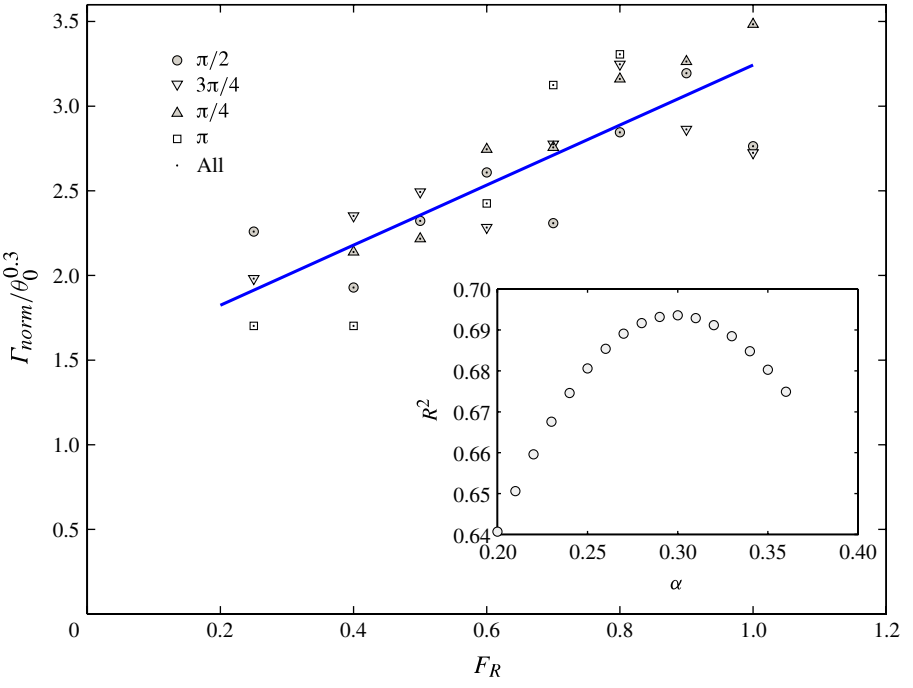


FIGURE 19. (Colour online) Scaled normalized circulation $\Gamma_{norm}/\theta_0^{0.3}$, with forcing amplitude θ_0, for frequency ratio $F_R \leqslant 1.0$. The inset plots the coefficient of determination R^2 against the amplitude scaling exponent α.

the cylinder surface moves in the same direction as the direction of roll up of the shear layer of the evolving vortex, the relative motion between the fluid and the solid surface gets diminished and then the range of surface motion (forcing amplitude) may not have significant contribution to the strength of the shed vortex.

To further investigate the detailed behaviour of the decay curve discussed above, a common curve fit to all circulation values for $F_R \geqslant 1.0$ was done and is also shown in figure 18. A power law of the form $CF_R^{-1.14}$ with constant $C = 3.31$ was found to provide an excellent fit ($R^2 = 0.98$) to the data. The behaviour of circulation at values of $F_R < 1.0$, however, is characterized by a dependency on the forcing amplitude. As is seen from the figure 19, a reasonably good linear fit ($R^2 = 0.69$) to the data for $F_R < 1.0$ can be obtained if the values of normalized circulation are further scaled by the forcing amplitude to the power of 0.3 suggesting the dependence of circulation values on F_R and θ_0 to be of the form $(D + EF_R)\theta_0^{0.3}$ where $D = 1.47$ and $E = 1.77$. To the best of the authors' knowledge, the existence of decay character of the shed vortex circulation in the region $F_R \geqslant 1.0$, independent of the forcing amplitude, and the scaling behaviour at $F_R < 1.0$ appear to be a new finding.

While the circulation variation described above was found for all amplitudes studied with forcing amplitudes $\geqslant \pi/4$, it does not apply for very small amplitudes, such as $\pi/8$. As shown in figure 18 (inset) the normalized circulation is now found to be essentially independent of the driving frequency, and its average value 2.54 was almost identical to the value of 2.53 for the no oscillation case measured in the present experiments. This is to be expected since reducing the oscillation amplitude to lower and lower values simulates a stationary cylinder. This can also be seen by examining

https://doi.org/10.1017/jfm.2013.469 Published online by Cambridge University Press

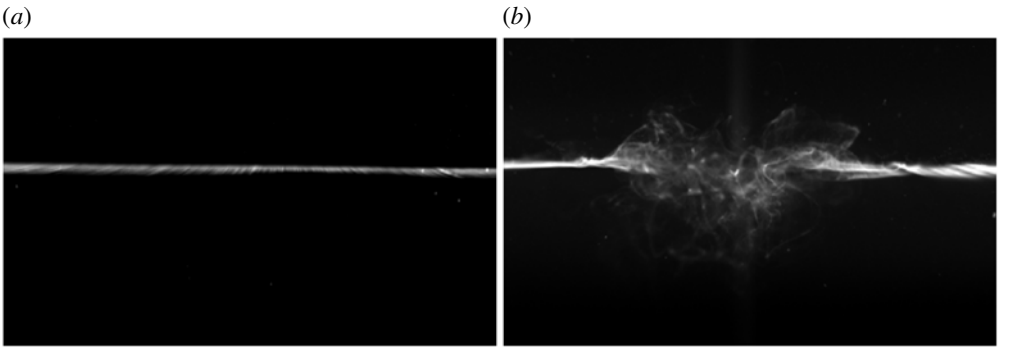


FIGURE 20. Illustration of the difference in two-dimensional and three-dimensional character of the flow as seen in the end-view flow visualization data. (*a*) Two-dimensional flow in the water tunnel test section with no cylinder. (*b*) Three-dimensional character of the flow in the far field of a cylinder with no oscillation at $Re = 400$.

the vorticity flux from the cylinder surface due to the two source terms present in the problem, namely, tangential surface acceleration and surface pressure gradient. The vorticity flux from the cylinder surface due to tangential surface acceleration is proportional to oscillation amplitude and square of the forcing frequency and therefore becomes vanishingly small as the oscillation amplitude tends to zero independent of the forcing frequency; however, the vorticity flux due to the pressure gradient effect tends to a value appropriate for a stationary cylinder ($\propto U_\infty^2/D$) in this limiting case.

3.3. *Flow visualization along the third dimension (end view)*

This part of the study was motivated by the following questions. To what extent is the wake structure shown by planar flow visualization in the previous sections two-dimensional? Does the wake behave in a two-dimensional manner or does it show three-dimensional character at certain forcing parameters? Can the wake be forced to become two-dimensional even in the far field when it is known to be highly three-dimensional? To answers such questions, flow visualization data was taken along the end view (see figure 2) at $Re = 185$ and 400 in both the near- and the far-field regions. The assumption was made that if the flow, in the plane of the hydrogen bubble sheet, is behaving in a two-dimensional manner then the bubble sheet would appear as a line (or an edge) in the end view and if the flow was three-dimensional then the bubbles would be advected due to the velocity component in the direction of cylinder axis and would be visible. It is in this sense, i.e. the absence of axial flow at the location of planar flow visualization plane that the word 'two-dimensional' should be interpreted in the present work. This flow visualization scheme would not give information on the detailed three-dimensional vortical structures but would certainly confirm if the flow is behaving in a two-dimensional manner in the visualization plane. Figure 20 illustrates this effect. Figure 20(*a*) shows the end view of the hydrogen bubble sheet in the water tunnel test section with no cylinder in place. The bubble sheet is visible as a line with no evidence of rising bubbles, clearly indicating that the flow is two-dimensional as expected. Figure 20(*b*) shows the end view of the far-field wake behind a stationary cylinder at Reynolds number of 400. The wake is known to be highly three-dimensional in these conditions and this is clearly evident in the figure 20(*b*) which shows a very mixed turbulent-like flow region made visible by bubbles advecting out of the bubble sheet plane. The flow visualizations were

https://doi.org/10.1017/jfm.2013.469 Published online by Cambridge University Press

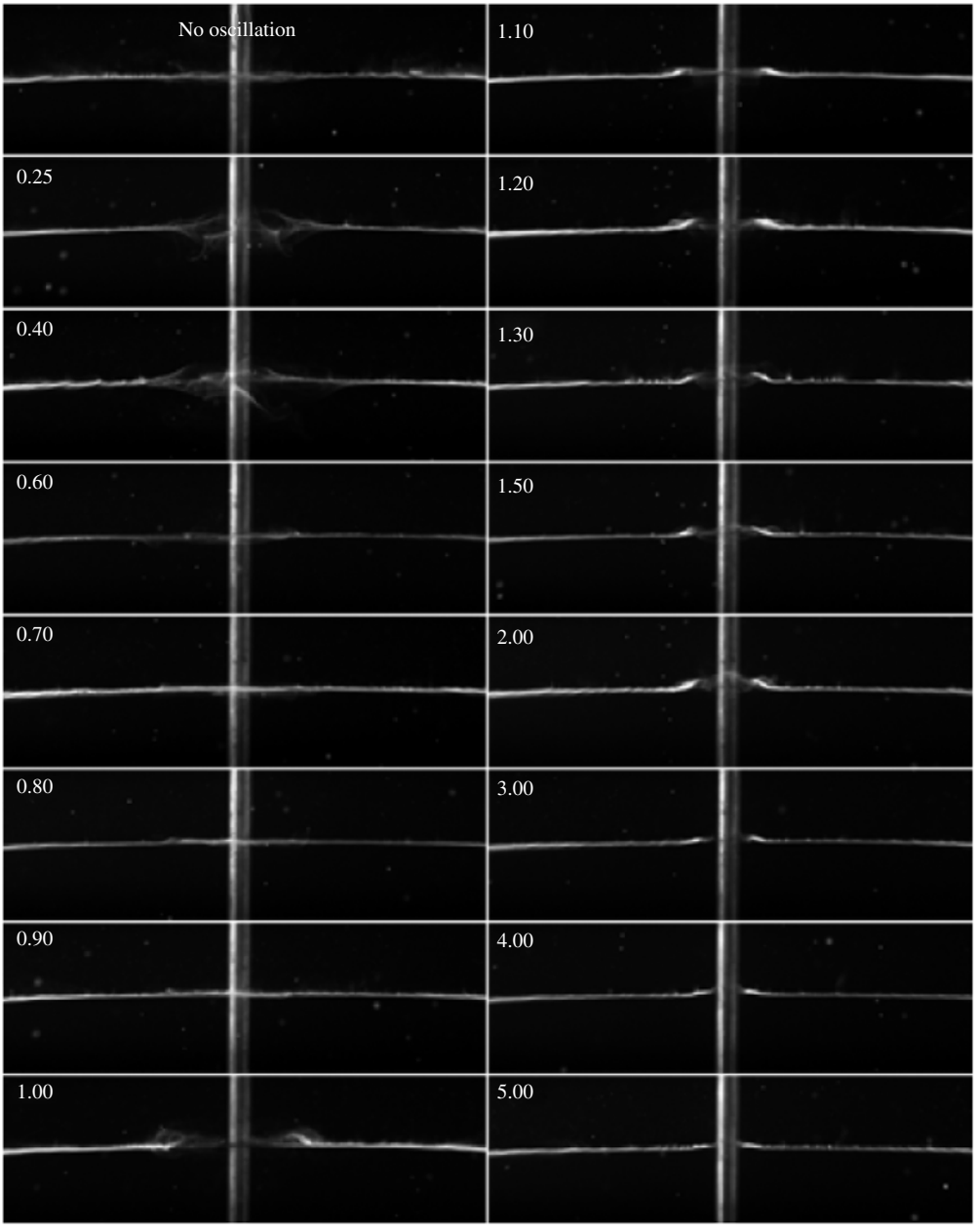


FIGURE 21. End view of the near-field wake structure at forcing amplitude of $\pi/2$ illustrating its almost two-dimensional character at $Re = 185$. The number on each frame represents the value of forcing frequency, F_R.

done both in the near field and the far field and were confined to the same spanwise location that was used for the wake structure visualizations in earlier sections.

The near-field wake structure at $Re = 185$ shows an almost two-dimensional character at all forcing parameters. Figure 21 shows this two-dimensional character, as an example, for a forcing amplitude of $\pi/2$. The bubble sheet is visible as a line

https://doi.org/10.1017/jfm.2013.469 Published online by Cambridge University Press

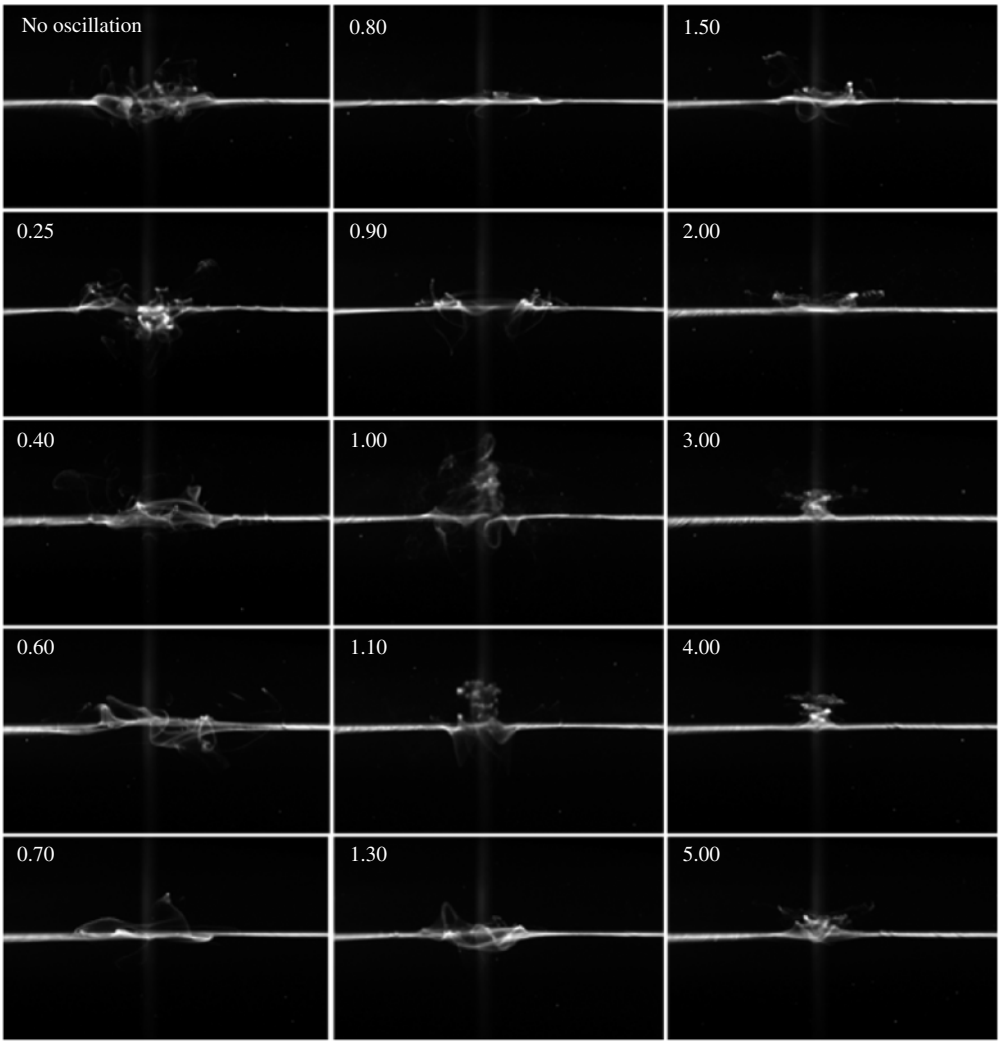


FIGURE 22. End view of the far-field wake structure at a forcing amplitude of $\pi/2$ and $Re = 185$. The number on each frame represents the value of the forcing frequency, F_R.

with evidence of small three-dimensional effects at lower forcing frequencies ranging from 0.25 to 0.40. The near-field wake appears to be almost two-dimensional at all forcing frequencies.

The end view of the far-field wake structure for forcing amplitude of $\pi/2$ is shown in figure 22. The figure shows that with no cylinder oscillation, the far-field wake exhibits three-dimensional effects at $Re = 185$ which get suppressed at $F_R = 0.7$ and 0.8. This is also the forcing frequency range where the shed vortex circulation reaches a maximum and there is complete lock-on at all downstream distances (see figures 18 and 8). In this forcing region the vortex street also appears to be well organized (in both the near and far field) with no signs of any unstable behaviour and with the vortex street looking very similar to that behind a stationary cylinder (see figures 6 and 7). This suggests that when the wake is completely locked-on or has vanishing absolutely unstable region (Thiria & Wesfreid 2007) then the three-dimensionalities

https://doi.org/10.1017/jfm.2013.469 Published online by Cambridge University Press

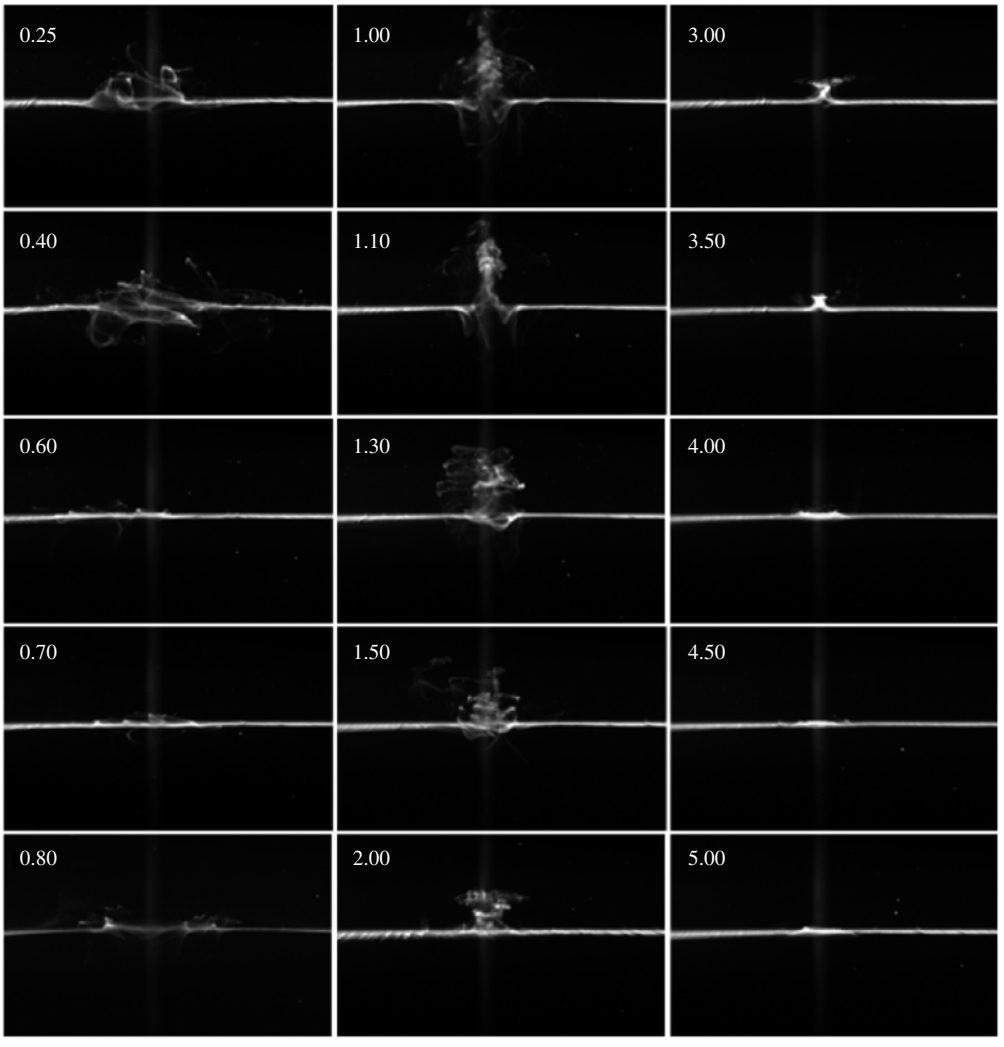


FIGURE 23. End view of the far-field wake structure at a forcing amplitude of $3\pi/4$ and $Re = 185$. The number on each frame represents the value of the forcing frequency, F_R.

tend to get suppressed. Figure 22 shows a sudden surge of advecting bubbles along the cylinder axis at $F_R \sim 1.0$ illustrating sudden rise in axial flow (three-dimensional effect). This effect was observed to be very repeatable. Examination of figure 6 shows that there is a change in mode shape around $F_R \sim 1.0$ leading to large separation between two rows of vortices (double row mode) with the vortices in the same row combining to form larger vortices in the far field. The end view visualization in figure 22 demonstrates that the combined processes of change in mode shape and vortex pairings giving rise to different near- and far-field wake structure coincides with the two-dimensional wake structure changing to a highly three-dimensional wake structure in the far field (see the end view in figure 22 at $F_R = 0.8$ and 1.0 for comparison). Jacono *et al.* (2010) showed, using Floquet stability analysis at $Re = 300$ and $F_R = 1.0$, that at larger oscillation amplitudes, such as $\pi/2$ in the present experiments, the wake becomes unstable to new three-dimensional mode (which they

https://doi.org/10.1017/jfm.2013.469 Published online by Cambridge University Press

called mode D). This instability arises after the suppression of mode A and mode B three-dimensional modes and as shown by Jacono *et al.* (2010), occurs when the near-wake transitions to a double-row mode starting almost from the cylinder location. The enhanced three-dimensional effect seen in the present experiments in the far wake when the wake mode transitions to a double-row mode is possibly the result of this new three-dimensional mode which can potentially develop even at $Re = 185$ with cylinder performing rotational oscillations. The enhanced three-dimensional effect in the far field shown in figure 22 slowly diminishes as the forcing frequency is increased as is shown by the decreasing height of bubbles advecting along the cylinder axis direction from $F_R = 1.1$ to 5.0.

Figure 23 shows the far-field end view of the wake structure for an oscillation amplitude of $3\pi/4$. The figure shows the three-dimensional character of the wake at lower forcing frequencies of 0.25 and 0.40. The wake becomes two-dimensional in forcing frequency range from $F_R \sim 0.6$ to 0.8. This is also the region where the circulation of the first detached vortex reaches a maximum (see figure 18). Near $F_R \sim 1.0$ there is a surge in flow along the axial direction resulting in enhanced three-dimensional effect. Forcing frequency range, $F_R \sim 0.8$–1.0, is the range in which the mode shape changes as can be seen from figures 9 and 10. Figure 23 shows that increased forcing results in diminishing axial flow and the wake behaves in a two-dimensional manner at higher frequencies such as $\sim F_R \geqslant 4.0$. The increased three-dimensional character due to mode shape change and vortex pairings and return to two-dimensionality at higher forcing frequencies was also observed in the end view images (not shown here) at all other oscillation amplitudes studied in the present study.

The effect of rotary oscillations forcing the flow to become two-dimensional in the far-field wake can have many applications such as in controlling fluid mixing and in some defense applications. To investigate whether the far-field wake can be made two-dimensional at higher Reynolds numbers, an attempt was made to examine only the end-view flow visualization images at a moderately high Reynolds number of 400. This was also the Reynolds number used by Poncet (2004) in his numerical studies to show that close to the cylinder (5–6D) the flow can be made two-dimensional using rotary oscillations at high enough forcing amplitude and frequency. Figure 24 shows the end view of the far-field wake structure at $Re = 400$ and forcing amplitude of $\pi/2$ for various values of forcing frequencies. It is clear from the figure that the wake is highly three-dimensional with no cylinder oscillation and also at low forcing frequencies ranging from $\sim F_R = 0.25$ to 2.0. Increasing the forcing frequency makes the flow two-dimensional as is clear from the end view images for $F_R \geqslant 2.5$ in figure 24 which shows the hydrogen bubble sheet as a line with no evidence of out-of-plane motion.

To study the dependence of such a control of wake structure on the forcing amplitude, end-view images of the wake structure were captured for forcing amplitudes of $\pi/8$, $\pi/4$, $\pi/2$, $3\pi/4$ and π at $Re = 400$. The end view of the wake structure for forcing amplitude of $\pi/4$ (not shown here) looked similar to that for forcing amplitude of $\pi/2$ shown in figure 24 except that the return to two-dimensionality occurred for $F_R \geqslant 3.5$. The forcing at amplitudes of $\pi/8$, $3\pi/4$ and π were not effective in making the flow two-dimensional in the far field in the range of forcing frequencies studied in the present work. Figure 25 shows the far-field wake structure in the end view at $Re = 400$ and forcing amplitude of $3\pi/4$. The figure clearly shows three-dimensional effects with no indication of return to two-dimensionality at all ranges of forcing frequencies studied. The wake structure

https://doi.org/10.1017/jfm.2013.469 Published online by Cambridge University Press

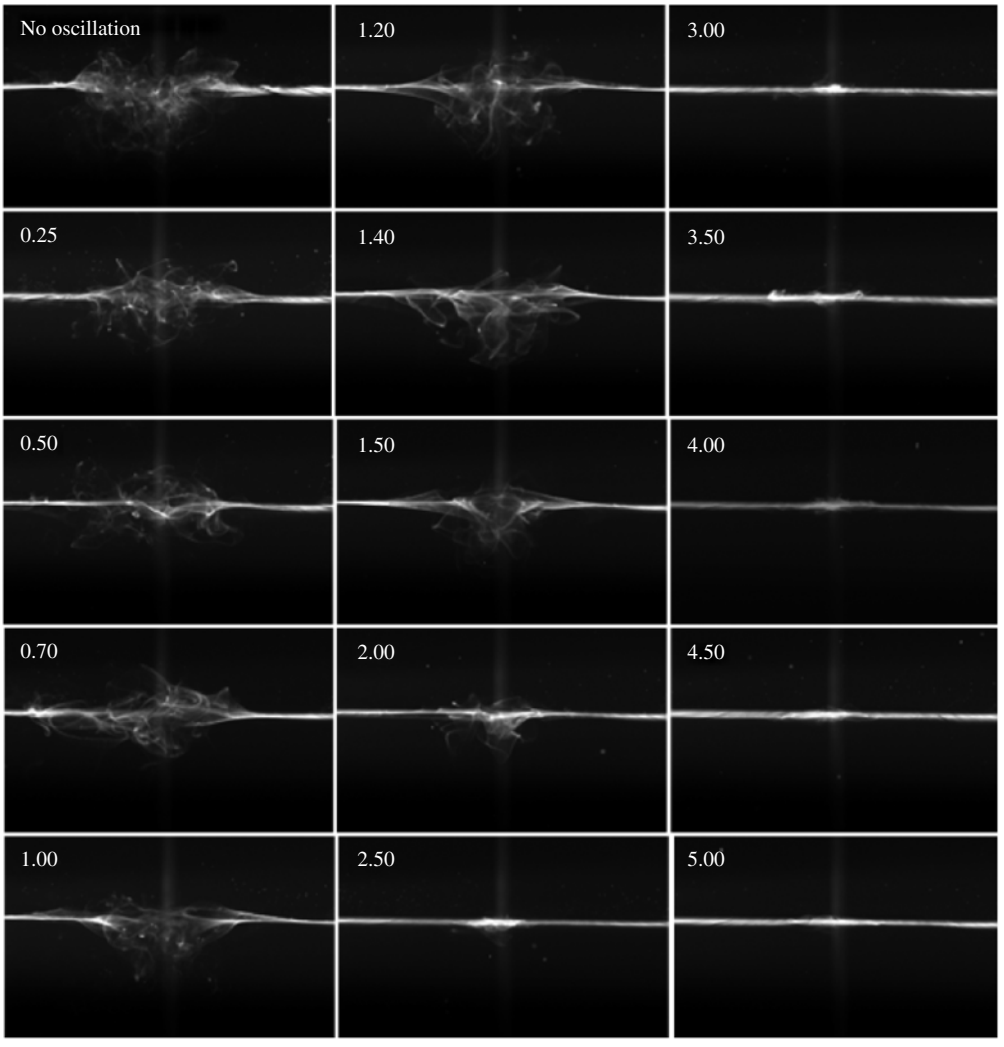


FIGURE 24. End view of the far-field wake structure at a forcing amplitude of $\pi/2$ at $Re = 400$ illustrating the wake structure becoming two-dimensional in the range $\sim F_R \geqslant 2.5$. The number on each frame represents the value of the forcing frequency, F_R.

in figure 25 is also representative of the wake structure observed for oscillation amplitudes of $\pi/8$ and π. This study examined five discrete amplitudes and showed that return to two-dimensionality occurs only at oscillation amplitudes of $\pi/4$ and $\pi/2$ and not above and below these two values. This suggests possibly that the rotary oscillations can force the flow in the far field at $Re = 400$ to become two-dimensional only in a range of forcing amplitudes ($\sim\pi/4 \leqslant \theta_0 \leqslant \pi/2$ in the present study) in the range of forcing frequencies studied. Poncet (2004) was the first investigator who numerically showed, for the first time, for the case of $F_R = 2.0$, that close to the cylinder ($\sim 0 \leqslant x/D \leqslant 6$) the flow can be forced to become two-dimensional above forcing amplitude, θ_0, of $\sim\pi/4$. The question of other values of F_R and the dynamics in the far field were left open in his work.

https://doi.org/10.1017/jfm.2013.469 Published online by Cambridge University Press

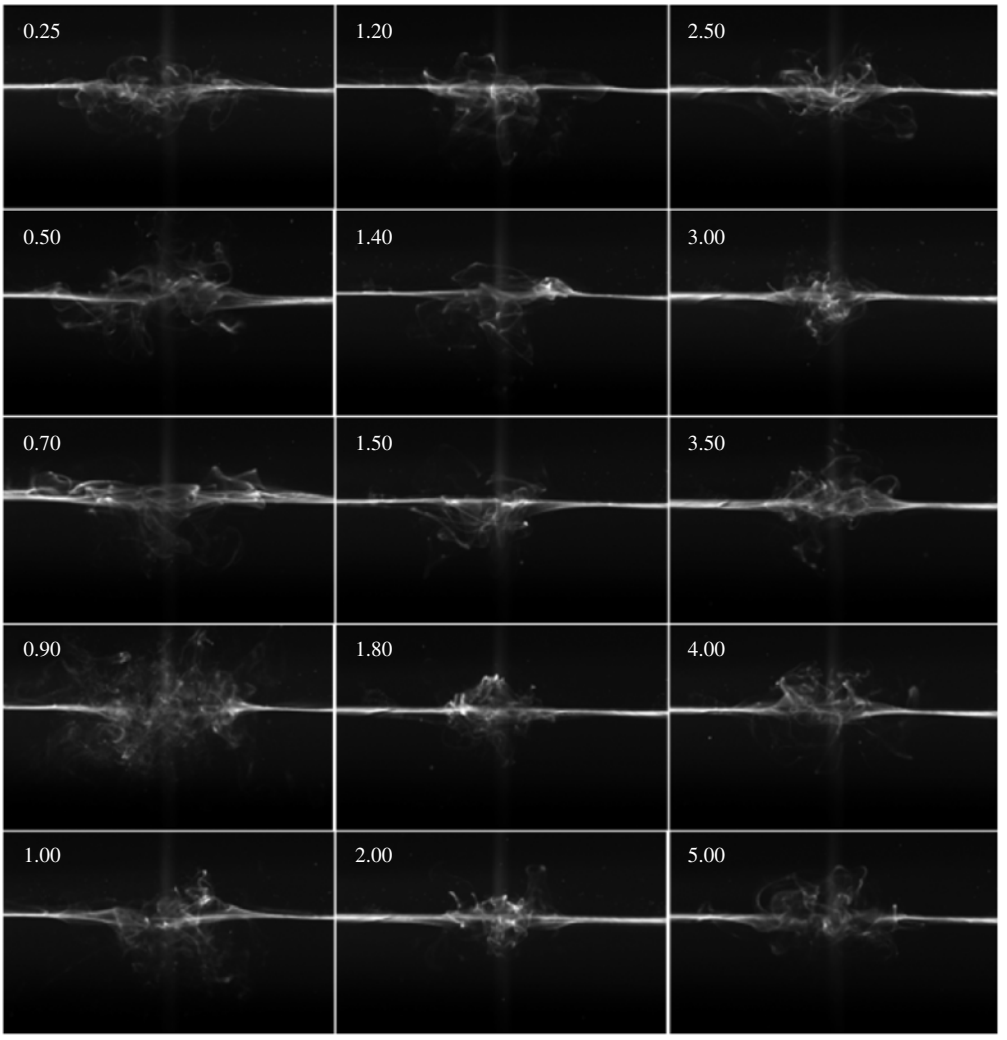


FIGURE 25. End view of the far-field wake structure at a forcing amplitude of $3\pi/4$ at $Re = 400$. The number on each frame represents the value of the forcing frequency, F_R.

The near-field wake structure showed interesting flow features in the end view at $Re = 400$ at certain forcing amplitudes. Figure 26 shows the wake structure for a forcing amplitude of $3\pi/4$. Comparison of figures 25 and 26 shows that mixing due to three-dimensional effects in the near-field region is substantially lower than in the far-field region. In addition, very organized 'tornado-like' flow features on either side of the cylinder are seen in the forcing frequency range, $\sim 0.9 \leqslant F_R \leqslant 1.5$ in figure 26. The structure of these features as seen in figure 26 suggests strong directed flow along the axial direction resulting in the bubbles of the hydrogen bubble sheet moving out of the plane in a spiral-shaped motion. The direction of this organized spiral motion is mostly seen in the downward direction in the present experiments; however, there is no reason why this motion cannot be upward and may be attributed to any kind of slight asymmetry in the end conditions of the experiment. A similar wake structure in the end view was observed for forcing amplitudes of $\pi/2$ and π; however, the range of

https://doi.org/10.1017/jfm.2013.469 Published online by Cambridge University Press

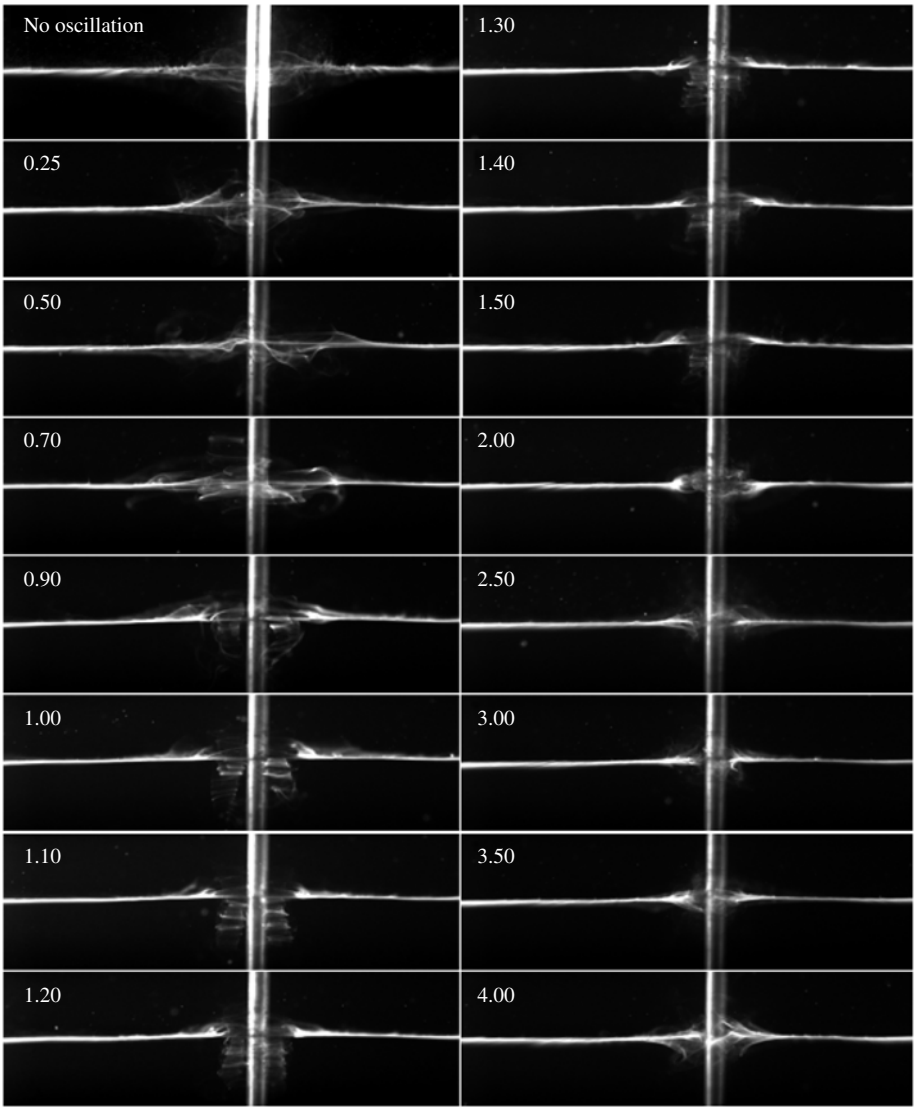


FIGURE 26. End view of the near-field wake structure at a forcing amplitude of $3\pi/4$ at $Re = 400$ illustrating 'tornado-like' flow features in the forcing frequency range, $\sim 0.9 \leqslant F_R \leqslant 1.5$. The number on each frame represents the value of the forcing frequency, F_R.

forcing frequencies where 'tornado-like' structures were seen was $\sim 1.0 \leqslant F_R \leqslant 1.5$ for $\theta_0 = \pi/2$ and $\sim 0.8 \leqslant F_R \leqslant 1.3$ for $\theta_0 = \pi$. At lower forcing amplitudes of $\pi/8$ and $\pi/4$ studied in the present work at $Re = 400$, no such flow features were observed. Similar study at lower Reynolds number of 185 did not reveal such flow features, suggesting that directed axial flow in the near-field region occurs at higher Re in a range of forcing frequencies and only above a threshold forcing amplitude.

The present experimental data illustrating the control of wake structure along the axial direction through rotary oscillations is new to the best of the authors' knowledge and appears to be a new contribution to the physics of the problem.

https://doi.org/10.1017/jfm.2013.469 Published online by Cambridge University Press

4. Conclusions

The wake structure resulting from flow past a rotationally oscillating cylinder is studied experimentally at $Re = 185$ using flow visualization, hot-wire anemometry and PIV. The oscillations amplitudes range from $\pi/8$ to π and forcing frequencies range from 0.25 to 5.0 times the Strouhal frequency. Rotary oscillations were observed to have significant effect on the wake structure depending on the forcing parameters. It is found that the lock-on of the wake to the forcing frequency depends not only on the forcing parameters but also the downstream distance from the cylinder. The lock-on region in the forcing-amplitude/forcing-frequency plane showed that the forcing frequency range in which the lock-on occurs at a given forcing amplitude decreases as downstream distance increases. The lower-frequency boundary of the lock-on region is fairly insensitive to the downstream location whereas the higher-frequency boundary depends strongly on the downstream distance. At higher forcing frequencies, the far-field wake decouples from the near-field wake and behaves similar to the wake behind a stationary cylinder. The vortex-shedding frequency in the far-field wake at $x/D = 23$ and higher forcing frequencies is observed to be smaller than the Strouhal frequency of a stationary cylinder by as much as $\sim$60 % depending on the forcing amplitude. The measurements of the circulation of the first detached vortex from the PIV data revealed a decay curve, independent of forcing amplitude for forcing frequencies greater than the Strouhal frequency. At smaller forcing frequencies the circulation scales with forcing amplitude as $\theta_0^{0.3}$.

The end-view visualization of the hydrogen bubble sheet showed that significant control of the flow can be achieved along the cylinder axis by subjecting the cylinder to rotational oscillations. In some cases, the flow can be forced to become two-dimensional (or planar) in the visualization plane at certain forcing parameters. The near-field visualization revealed that the flow field is almost planar at $Re = 185$; however, in the far field, strong three-dimensional effects are seen to emerge at forcing parameters where the wake mode changes by sudden increase in the separation of the two rows of shed vortices. This was demonstrated for forcing amplitudes of $\pi/2$ and $3\pi/4$ near $F_R \sim 1.0$. It was also seen in the far field at $Re = 185$ that the flow became planar when the forcing frequency was close to the value at which the circulation of the shed vortices reaches maximum. This was seen in figure 23 for a forcing amplitude of $3\pi/4$ where the flow was seen to become planar near $F_R \sim 0.6$–0.7.

The visualization data also showed clearly that for $Re = 400$ the far-field flow can be made planar at higher forcing frequencies ($\sim F_R \geqslant 2.5$) only for a range of forcing amplitudes. In the present experiments it was found that such a control can be achieved only at forcing amplitudes of $\pi/4$ and $\pi/2$. The near-field flow visualization at $Re = 400$ showed the presence of a strongly directed axial flow resulting in 'tornado-like' flow features only at forcing amplitudes of $\pi/2$ and higher.

Acknowledgements

The authors would like to acknowledge the support provided by the National Science Foundation through the MRI grant CMMI-0723094 which made the purchase of the PIV system possible. The help of the machinist Mr A. Sacco in machining some of the experimental components is gratefully acknowledged. S.K. would like to acknowledge the support provided by the O. Vasquez Raña fellowship from the University of Texas at Brownsville, and O.P. gratefully acknowledges support from Tecnológico de Monterrey through the Research Chair for Wind Energy (contract no.

https://doi.org/10.1017/jfm.2013.469 Published online by Cambridge University Press

CAT158). Finally, the suggestions of the referees were very helpful in improving the paper.

Supplementary movies

Supplementary movies are available at http://dx.doi.org/10.1017/jfm.2013.469.

REFERENCES

BADR, H. M. & DENNIS, S. C. R. 1985 Time-dependent viscous flow past an impulsively started rotating and translating circular cylinder. *J. Fluid Mech.* **158**, 447–488.

BAEK, S.-J. & HYUNG, J. S. 1998 Numerical simulation of the flow behind a rotary oscillating circular cylinder. *Phys. Fluids* **10** (4), 869–876.

BEARMAN, P. W. 1984 Vortex shedding from oscillating bluff bodies. *Annu. Rev. Fluid Mech.* **16**, 195–222.

BERGER, E. & WILLIE, R. 1972 Periodic flow phenomenon. *Annu. Rev. Fluid Mech.* **4**, 313–340.

BERGMANN, M., CORDIER, L. & BRNACHER, J.-P. 2006 On the generation of a reverse von Kármán street for the controlled cylinder wake in the laminar regime. *Phys. Fluids* **18**, 028101.

BISHOP, R. E. D & HASSAN, A. Y. 1964 The lift and drag forces on a circular cylinder oscillating in a flowing fluid. *Proc. R. Soc. Lond. Ser.* A **227**, 51–75.

CHENG, M., CHEW, T. & LUO, S. C. 2001 Numerical investigation of a rotationally oscillating cylinder in mean flow. *J. Fluids Struct.* **15**, 981–1007.

CHOI, S., CHOI, H. & KANG, S. 2002 Characteristics of flow over a rotationally oscillating cylinder at low Reylonds number. *Phys. Fluids* **14** (8), 2767–2777.

CHYU, C., LIN, J.-C, SHERIDAN, J. & ROCKWELL, D. 1995 Kármán vortex formation from a cylinder: role of phase-locked Kelvin–Helmholtz vortices. *Phys. Fluids* **7** (9), 2288–2290.

CHYU, C. K. & ROCKWELL, D. 1996 Near wake structure of an oscillating cylinder: effect of controlled shear layer vortices. *J. Fluid Mech.* **322**, 21–49.

CIMBALA, J. M., NAGIB, H. M & ROSHKO, A. 1988 Large structure in the far wakes of two-dimensional bluff bodies. *J. Fluid Mech.* **190**, 265–298.

DENG, J., SHAO, X.-M. & REN, A.-L. 2007 Vanishing of three-dimensionality in the wake behind a rotationally oscillating circular cylinder. *J. Hydrodyn.* **19** (6), 751–755.

DENNIS, S. C. R., NGUYEN, P. & KOCABIYIK, S. 2000 The flow induced by a rotationally oscillating and translating circular cylinder. *J. Fluid Mech.* **407**, 123–144.

FILLER, J. R., MARSTON, P. L & MIH, W. C. 1991 Response of the shear layers separating from a circular cylinder to small-amplitude rotational oscillations. *J. Fluid Mech.* **231**, 481–499.

FUJISAWA, N., KAWAJI, Y. & IKEMOTO, K. 2001 Feedback control of vortex shedding from a circular cylinder by rotational oscillations. *J. Fluids Struct.* **15**, 23–37.

FUJISAWA, N., TANAHASHI, S. & SRINIVAS, K. 2005 Evaluation of pressure field and fluid forces on a circular cylinder with and without rotational oscillation using velocity data from PIV measurement. *Meas. Sci. Technol.* **16**, 989–996.

GRIFFIN, O. M. & RAMBERG, S. E. 1976 Vortex shedding from a circular cylinder vibrating in line with an incipient uniform flow. *J. Fluid Mech.* **75**, 257–271.

GU, W., CHYU, C. & ROCKWELL, D. 1994 Timing of vortex formation from an oscillating cylinder. *Phys. Fluids* **6** (11), 3677–3682.

HE, J.-W., GLOWINSKI, R., METCALFE, R., NORDLANDER, A. & PERIAUX, J. 2000 Active control and drag optimization for flow past a circular cylinder. I. Oscillatory cylinder rotation. *J. Comput. Phys.* **163**, 83–117.

HOURIGAN, K., THOMPSON, M. C., SHEARD, G. J., RYAN, K., LEONTINI, J. S. & JOHNSON, S. A. 2007 Low Reynolds number instabilities and transitions in bluff body wakes. *J. Phys.: Conf. Ser.* **64**, 012018.

HURLBUT, S. E., SPAULDING, M. L. & WHITE, F. M. 1982 Numerical solution for laminar two-dimensional flow about a cylinder oscillating in a uniform stream. *ASME J. Fluids Engng* **104**, 214–220.

https://doi.org/10.1017/jfm.2013.469 Published online by Cambridge University Press

JACONO, D. L., LEONTINI, J. S., THOMPSON, M. C. & SHERIDAN, J. 2010 Modifications of three-dimensional transition in the wake of a rotationally oscillating cylinder. *J. Fluid Mech.* **643**, 349–362.

VON KÁRMÁN, T. 1911 Über den Mechanismus des Widerstands, den ein bewegter Körper in einer Flüssigkeit erfährt. *Göttinger Nachrichten, Math. Phys. Kl.* 509–517.

VON KÁRMÁN, T. 1912 Über den Mechanismus des Widerstands, den ein bewegter Körper in einer Flüssigkeit erfährt. *Göttinger Nachrichten, Math. Phys. Kl.* 547–556.

KONSTANTINIDIS, E., BALABANI, S. & YIANNESKIS, M. 2005 Conditional averaging of PIV plane wake data using a cross-correlation approach. *Exp. Fluids* **39** (1), 38–47.

KUMAR, S., CANTU, C. & GONZALEZ, B. 2011*b* Flow past a rotating cylinder at low and high rotation rates. *ASME J. Fluids Engng* **133**, 041201.

KUMAR, S., GONZALEZ, B. & PROBST, O. 2011*a* Flow past two rotating cylinders. *Phys. Fluids* **23**, 014102.

KUMAR, S., LAUGHLIN, G. & CANTU, C. 2009 Near-wake structure behind two circular cylinders in a side-by-side configuration with heat release. *Phys. Rev.* E **80**, 066307.

LAMB, H. 1932 *Hydrodynamics*, 6th edn, pp. 224–229. Dover.

LEE, S. & LEE, J. 2006 Flow structure of a wake behind a rotationally oscillating circular cylinder. *J. Fluids Struct.* **22**, 1097–1112.

LEE, S.-J. & LEE, J.-Y. 2008 PIV measurements of the wake behind a rotationally oscillating circular cylinder. *J. Fluids Struct.* **24**, 2–17.

LU, M.-Y. & SATO, J. 1996 A numerical study of flow past a rotationally oscillating cylinder. *J. Fluids Struct.* **10**, 829–849.

LU, L., QIN, J.-MIN, B. TENG & LI, Y.-CHENG 2011 Numerical investigations of lift suppression by feedback rotary oscillation of circular cylinder at low Reynolds number. *Phys. Fluids* **23**, 033601.

MAHFOUZ, F. M. & BADR, H. M. 2000 Flow structure in the wake of a rotationally oscillating cylinder. *ASME J. Fluids Engng* **122**, 290–301.

NAZARINIA, M., LO JOCONO, D., THOMSON, M. C. & SHERIDAN, J. 2009 The three-dimensional wake of a cylinder undergoing a combination of translational and rotational oscillation in a quiescient fluid. *Phys. Fluids* **21**, 064101.

NEGRI, M., COZZI, F. & MALAVASI, S. 2011 Self-synchronized phase averaging of PIV measurements in the base region of a rectangular cylinder. *Meccanica* **46** (2), 423–435.

OKAJIMA, A., TAKATA, H. & ASANUMA, T. 1975 Viscous flow around a rotationally oscillating circular cylinder. *Inst. Space Aero. Sci. Rep.* 532, University of Tokyo.

PONCET, P. 2002 Vanishing of mode B in the wake behind a rotationally oscillating circular cylinder. *Phys. Fluids* **14** (7), 2073–2087.

PONCET, P. 2004 Topological aspects of three-dimensional wakes behind rotary oscillating cylinders. *J. Fluid Mech.* **517**, 27–53.

PRANDTL, L. 1925 *Die Naturwissenschaften*, **13**, pp. 93–108. (English translation: Applications of the Magnus effect to the wind propulsion of ships. NACA Tech. Mem. 387, June (1926).).

PRASAD, A. & WILLIAMSON, C. H. K. 1997 The instability of the shear layer separating from a bluff body. *J. Fluid Mech.* **333**, 375–402.

PROTAS, B. & WESFREID, J. E. 2002 Drag force in the open-loop control of the cylinder wake in the laminar regime. *Phys. Fluids* **14** (2), 810–826.

SHIELS, D. & LEONARD, A. 2001 Investigation of a drag reduction on a circular cylinder in rotary oscillation. *J. Fluid Mech.* **431**, 297–322.

TANEDA, S. 1978 Visual observations of the flow past a circular cylinder performing a rotary oscillation. *J. Phys. Soc. Japan* **45** (3), 1038–1043.

TANIDA, Y., OKAJIMA, A. & WATANABE, Y. 1973 Stability of the circular cylinder oscillating in a uniform flow or in a wake. *J. Fluid Mech.* **61**, 769–784.

THIRIA, B., GOUJON-DURAND, S. & WESFREID, J. E. 2006 The wake of a cylinder performing rotary oscillations. *J. Fluid Mech.* **560**, 123–147.

THIRIA, B. & WESFREID, J. E. 2007 Stability properties of forced wakes. *J. Fluid Mech.* **579**, 137–161.

https://doi.org/10.1017/jfm.2013.469 Published online by Cambridge University Press

TOKUMARU, P. T. & DIMOTAKIS, P. E. 1991 Rotary oscillation control of a cylinder wake. *J. Fluid Mech.* **224**, 77–90.

TOKUMARU, P. T. & DIMOTAKIS, P. E. 1993 The lift of a cylinder executing rotary motions in a uniform flow. *J. Fluid Mech.* **255**, 1–10.

WEI, T. & SMITH, C. R. 1986 Secondary vortices in the wake of circular cylinders. *J. Fluid Mech.* **169**, 513–533.

WEIHS, D. 1972 Semi infinite vortex trails, and their relation to oscillating aerofoils. *J. Fluid Mech.* **54**, 679–690.

WILLIAMSON, C. H. K. 1996 Vortex dynamics in the cylinder wake. *Annu. Rev. Fluid Mech.* **28**, 477–539.

WILLIAMSON, C. H. K & ROSHKO, A. 1988 Vortex formation in the wake of an oscillating cylinder. *J. Fluids Struct.* **2**, 355–381.

https://doi.org/10.1017/jfm.2013.469 Published online by Cambridge University Press